Report L-910900-13

Nuclear Light Bulb Propellant Heating Simulation Using a Tungsten/Argon Aerosol and Radiation from a DC Arc Surrounded by a Segmented Mirror Cavity

NASA Contract No. SNPC-70

UNITED AIRCRAFT CORPORATION

United Aircraft Research Laboratories

EAST HARTFORD, CONNECTICUT

United Aircraft Research Laboratories

UNITED AIRCRAFT CORPORATION

EAST HARTFORD, CONNECTICUT 06108

Report L-910900-13

Nuclear Light Bulb Propellant Heating
Simulation Using a Tungsten/Argon
Aerosol and Radiation from a DC Arc
Surrounded by a Segmented Mirror Cavity

NASA Contract No. SNPC-70

REPORTED BY John F. Klein
John F. Klein

APPROVED BY James W. Clark
James W. Clark, Chief
Fluid and Systems Dynamics

DATE September 1972

NO. OF PAGES 57

COPY NO. 28

FOREWORD

An exploratory experimental and theoretical investigation of gaseous nuclear rocket technology was conducted by the United Aircraft Research Laboratories under Contract SNPC-70 with the joint AEC-NASA Space Nuclear Systems Office. The Technical Supervisors of the Contract for NASA were Captain C. E. Franklin (USAF) of SNSO for the initial portion of the Contract performance period, and Dr. Karlheinz Thom of SNSO and Mr. Herbert J. Heppler of the NASA Lewis Research Center for the final portions. The following nine reports (including the present report) comprise the required Final Technical Report under the Contract:

1. Roman, W. C. and J. F. Jaminet: Development of RF Plasma Simulations of In-Reactor Tests of Small Models of the Nuclear Light Bulb Fuel Region. United Aircraft Research Laboratories Report L-910900-12, September 1972.

2. Klein, J. F.: Nuclear Light Bulb Propellant Heating Simulation Using a Tungsten-Particle/Argon Aerosol and Radiation from a DC Arc Surrounded by a Segmented Mirror Cavity. United Aircraft Research Laboratories Report L-910900-13, September 1972. (Present Report)

3. Jaminet, J. F.: Development of a Model and Test Equipment for Cold-Flow Tests at 500 Atm of Small Nuclear Light Bulb Configurations. United Aircraft Research Laboratories Report L-910900-14, September 1972.

4. Kendall, J. S. and R. C. Stoeffler: Conceptual Design Studies and Experiments Related to Cavity Exhaust Systems for Nuclear Light Bulb Configurations. United Aircraft Research Laboratories Report L-910900-15, September 1972.

5. Rodgers, R. J. and T. S. Latham: Analytical Design and Performance Studies of the Nuclear Light Bulb Engine. United Aircraft Research Laboratories Report L-910900-16, September 1972.

6. Latham, T. S. and R. J. Rodgers: Analytical Design and Performance Studies of Nuclear Furnace Tests of Small Nuclear Light Bulb Models. United Aircraft Research Laboratories Report L-910900-17, September 1972.

7. Krascella, N. L.: Spectral Absorption Coefficients of Argon and Silicon and Spectral Reflectivity of Aluminum. United Aircraft Research Laboratories Report L-910904-3, September 1972.

8. Palma, G. E.: Measurements of the UV and VUV Transmission of Optical Materials During High-Energy Electron Irradiation. United Aircraft Research Laboratories Report L-990929-3, September 1972.

9. Kendall, J. S.: Investigation of Gaseous Nuclear Rocket Technology -- Summary Technical Report. United Aircraft Research Laboratories Report L-910905-13, September 1972.

Report L-910900-13

Nuclear Light Bulb Propellant Heating Simulation Using a Tungsten/Argon Aerosol and Radiation from a DC Arc Surrounded by a Segmented Mirror Cavity

TABLE OF CONTENTS

Report L-910900-13

Nuclear Light Bulb Propellant Heating Simulation Using a Tungsten/Argon Aerosol and Radiation from a DC Arc Surrounded by a Segmented Mirror Cavity

SUMMARY

Further experiments were conducted to simulate radiant heating of the propellant stream of a nuclear light bulb engine. As in previous experiments, the primary objective was to obtain high bulk exit temperatures in the flowing simulated propellant stream by absorption of large fractions of the incident thermal radiation.

A high-power, vortex-stabilized dc arc within an uncooled fused silica tube was used as the radiant energy source. It was surrounded by a mirror system to increase the radiation incident on the simulated propellant. The 12.7-cm-long by 2.3-cm-wide, diverging-duct test section had a transparent front wall and a reflecting rear wall. The central stream of seeded gas, a tungsten-particle/argon aerosol, had unseeded argon buffer layers on both sides to prevent coating of the duct walls. Arc operating times were approximately 0.5 sec with power levels up to 780 kW. Bulk exit temperatures were measured using a calorimeter downstream of the duct.

To reach higher exit temperatures than those obtained previously, the following changes were made in the arc and mirror cavity during the present program: (1) the maximum dc arc power was increased by operating the power supplies at an overload condition and (2) an improved water-cooled segmented mirror cavity was developed to replace the previous cylindrical cavity. These two changes resulted in a factor of two increase in the radiation incident on the simulated propellant. In addition, a tungsten-particle/argon aerosol was used instead of the carbon-particle/argon aerosol, with expected benefits in terms of higher seed melting and boiling points and higher opacity in the vapor state. The latter change required development of a unique new tungsten powder feeder.

The maximum simulated propellant bulk exit temperature obtained was 4515°K, compared with 3860°K in previous tests, 3300 to 3700°K expected in in-reactor tests in the Nuclear Furnace, and 6660°K in the reference nuclear light bulb engine. The maximum temperature in these tests was limited primarily by the amount of radiation incident on the test section (determined by the arc operating characteristics and the effectiveness of the mirror cavity).

The highest bulk exit temperatures obtained were within 5 percent of the equivalent black-body temperatures of the radiation incident on the test section. In the nuclear light bulb reference engine design, it is assumed that the maximum propellant temperature will be 80 percent of the equivalent black-body radiating temperature of the fuel. Therefore, the present results suggest that it may be possible to obtain higher propellant temperatures for the same engine power in the reference engine.

For most tests, the duct walls protected by the buffer layers remained relatively clean. Examinations of deposits which occurred in a few of the high-power tests suggested that at least some tungsten vapor was present in the test section. With continued improvement of the dc arc and mirror cavity, it appears feasible to reach bulk exit temperatures of at least 5200°K where significant amounts of tungsten vapor are expected.

RESULTS AND CONCLUSIONS

1. Simulated propellant bulk exit temperatures up to 4515°K were obtained by absorption of thermal radiation from a dc arc. The simulated propellant was argon seeded with submicron-sized tungsten particles. The maximum temperature in these experiments was limited primarily by the amount of arc radiation incident on the test section which, in turn, was determined by the arc operating characteristics and the effectiveness of the segmented mirror cavity.

2. For most tests, there were no visible deposits on the duct walls protected by the buffer layers. Examinations of deposits which occurred in a few of the high-power tests suggested that at least some tungsten vapor was present in the test section. Time limitations on this program did not permit measurements to be made of the amount of radiation absorbed by these wall deposits, and did not permit complete investigation of changes that could be made in the buffer layers to attempt to reduce the deposits.

3. In preparation for these tests, changes were made in the dc arc operating procedure and in the vortex flow which resulted in substantial increases in the radiation incident on the simulated propellant relative to the levels available in previous tests. Operating the arc power supplies at an overload condition for the short 0.5-sec test time, the maximum arc power was increased from 480 to 780 kW, and the maximum radiation in the 12.7-cm length adjacent to the test section was increased from 238 to 322 kW. When combined with the mirror improvements mentioned below, these increases resulted in an increase in the maximum radiation incident on the simulated propellant stream from 34 to about 67 kW.

4. A segmented mirror cavity was developed to focus the dc arc radiation on the propellant heating test section. Mirror fabrication and cooling techniques were developed which prevented deterioration of mirror reflectivity previously experienced in regions of high heat flux. The ratio of radiation incident on the simulated propellant stream with the mirror to that without the mirror was about 2.2, compared with 1.4 in tests with the cylindrical mirror previously used.

5. To provide the required high weight flow rates of submicron-sized tungsten particles, a unique new high-pressure rotating drum powder feeder was developed. The feeder provides a flow of tungsten in argon carrier gas at tungsten weight flow rates up to 26 g/sec. It was operated at drum pressures up to 29 atm in tests of orifices for seed deagglomeration.

6. With continued improvement of the dc arc and mirror cavity, it appears feasible to reach bulk exit temperatures of at least 5200°K, where significant amounts of tungsten vapor are expected. It is estimated that the necessary increase in the radiation incident on the simulated propellant can be obtained primarily by (1) a

small increase in the power at which the arc is operated and (2) a change in the mirror design to make use of arc radiation from the ends of the arc outside the 12.7-cm test section length (the arc length is 17.78 cm). Further experiments with the unseeded buffer layers may also be beneficial.

INTRODUCTION

An experimental and theoretical investigation of gaseous nuclear rocket technology has been conducted by the United Aircraft Research Laboratories (UARL) under Contract SNPC-70 administered by the joint AEC-NASA Space Nuclear Systems Office. The overall research program is presently directed toward investigating the feasibility of the nuclear light bulb engine. This report discusses the portion of the research program in which the feasibility of heating propellants by thermal radiation is being investigated. In particular, it presents the results of tests in which a seeded simulated propellant, a tungsten-particle/argon aerosol, was heated to high bulk temperatures by absorption of thermal radiation from a dc arc radiant energy source.

Nuclear Light Bulb Concept and Reference Engine Configuration

The nuclear light bulb concept described in Refs. 1 and 2 is based on the principle of transfer of energy by thermal radiation from a fissioning gaseous nuclear fuel to seeded hydrogen propellant flowing through an annulus surrounding the nuclear fuel. Radiant energy is transferred through an internally cooled transparent wall which separates the nuclear fuel from the propellant stream. Figure 1(a) illustrates this principle of operation with a cross-section of one unit cavity. The reference engine (Ref. 3) is formed by a cluster of seven such cavities to increase the effective radiating surface area of the nuclear fuel cloud. Figure 1(b) is a schematic of the dc arc radiant energy source used in the propellant heating simulation tests. The significant dimensions of both the unit cavity and the propellant heating configuration are indicated. Figure 2 is a sketch showing additional detailed dimensions of one unit cavity of the reference engine. One-half of the rotationally symmetric cavity is shown. The propellant region is a divergent annulus, 1.8-m long with a 0.49-m inside diameter. The annulus width increases uniformly from 0.013 m at the inlet to 0.161 m at the exhaust.

In the reference engine, approximately 98 percent of the total thermal radiation incident on the propellant stream is calculated to be absorbed by the hydrogen propellant (Ref. 3). Hydrogen is essentially transparent to thermal radiation at the engine operating pressure of 500 atm and below a temperature of approximately 7780°K. Therefore, a seed material must be added to the propellant stream to provide the required opacity. The ideal seed material would consist of nonreactive, high-melting-point, high-boiling-point, submicron-sized metal particles that exhibit good absorption characteristics in both the particle and vapor forms. Submicron-sized particles, low-ionization-potential metal vapors, and various polyatomic gases have been examined theoretically and experimentally as possible seed materials for the propellant stream (Refs. 4 through 12). Submicron-sized solid or liquid particles exhibit essentially continuous spectral absorption characteristics as contrasted with discrete spectral absorption characteristics exhibited by low-ionization-potential metal vapors and polyatomic gases. Theoretical studies (Refs. 4 through 8) of

the absorption properties of small solid particles have been based on the Mie theory (Ref. 13). This theory describes the spectral extinction, absorption, and scattering of radiation by spherical particles as functions of particle size, material properties, and the wavelength of the incident radiation. The results of these stuides indicate that tungsten is attractive as a seed material because of its high melting point, high boiling point, and low reactivity with hydrogen. In the reference engine, nominal 0.05-micron-diam tungsten particles are assumed to be used as a propellant seed material.

In each unit cavity, the inner wall of the propellant annulus is highly transparent. The outer wall is highly reflective to reduce the heat load to the moderator and to increase the effective radiant energy path length in the propellant region. A thin layer of unseeded gas flows adjacent to both the inner and the outer walls of the propellant region. These thin unseeded layers serve as buffer regions which prevent the degradation of the optical properties of the walls due to coating by the propellant seed. They also aid in keeping hot gases away from the walls, thus reducing the heat transfer to the duct walls.

Principal Objectives

The principal objectives of this portion of the nuclear light bulb research program are:

(1) to experimentally demonstrate the heating of a simulated propellant to bulk exit temperatures greater than 4445°K (or 8000°R) by the absorption of thermal radiation (3860°K was achieved in previous tests; Ref. 14);

(2) to use a flow configuration similar to that of the nuclear light bulb engine in the sense of providing simulated propellant opacity with micron-sized solid particle tungsten seeds, which are separated from the propellant duct walls by buffer layers of unseeded gas; also, for some tests the walls of the propellant duct would be divergent and have a reflector on the rear wall; and

(3) to develop methods for feeding dispersing, deagglomerating and introducing the tungsten seed into the simulated propellant flow.

Experimental Approach

An experimental approach was developed based on (1) the need to provide sufficient simulated propellant opacity at high temperatures to absorb large percentages of incident radiation and (2) the need for increased radiation incident on the test section. These two major items were required to achieve the principal objectives.

To provide sufficient simulated propellant opacity at high temperatures, tungsten powder was used as the seed. It has higher melting and boiling points than the carbon seed used in earlier tests as well as increased opacity in the vapor state. It is the seed material selected for use in the reference nuclear light bulb engine.

Use of tungsten seed required the development of a tungsten seeder system which would provide the high flow rates of tungsten (>5 g/sec) estimated to be required for sufficient opacity during the simulated propellant heating tests. Also, cold-flow tests were required to identify an inlet and buffer flow configuration suitable for tests with tungsten particles. The flow configuration was approached through the use of a rectangular duct and inlet similar to those used in Ref. 14. However, provisions were made for a duct which had diverging walls and a reflector on the rear duct wall.

Two avenues were explored for increased radiation incident on the test section. First, tests were conducted to determine whether the dc arc could be operated at higher powers than in the tests reported in Ref. 14 (480 kW). These tests explored operating the power supplies at a higher short-term overload than in the past and changing both the dc arc argon flow rate and vortex injection angle. Second, tests of segmented mirror cavities for focusing dc arc radiation on the test section using uncooled aluminized-glass front surface mirrors were conducted at low arc powers (up to 100 kW). Based on these tests, a highly water-cooled segmented mirror cavity, capable of operation with the dc arc at maximum power (780 kW), was fabricated for the simulated propellant heating tests.

Results of the powder feeder development, cold-flow tests, dc arc modification, and segmented mirror cavity tests were combined in the simulated propellant heating tests. The main text of this report is divided into separate sections entitled DC ARC RADIANT ENERGY SOURCE, COLD-FLOW TESTS , and SIMULATED PROPELLANT HEATING TESTS . Details of the powder feeder development are presented in APPENDIX A.

DC ARC RADIANT ENERGY SOURCE

Objective

The objective of the dc arc test series was to increase the amount of radiation available over the levels used in previous simulated propellant heating tests. To satisfy this objective, the UARL dc arc heater operating power was increased from 480 to 780 kW for short test times (0.5 sec). The results of these tests and a brief description of the techniques used to measure arc radiation are presented in this portion of the report. Descriptions of the dc arc electrical components, configuration, electrodes, vortex system, gas and water cooling systems, and starting and control systems were given in APPENDIX A of Ref. 14 and are not included in this report.

Radiation Measurements

Configuration

Figure 3 shows a sketch of the basic dc arc and radiometer optical system. The 1-atm argon arc was vortex stabilized and was enclosed within a 4.0-cm-i.d., uncooled, fused silica tube. The arc was struck between a thoriated tungsten cathode and a magnetically augmented, water-cooled, copper anode. The anode-to-cathode distance was 17.78 cm.

As shown in Fig. 3, total radiation measurements were made of the power radiated from the dc arc column using a radiometer which incorporated a barium fluoride (BaF_2) thermopile detector. This arrangement of the thermopile and aperture allowed the radiometer to view a section of the dc arc column which was 2.55-cm high and wider than the diameter of the fused silica tube enclosing the dc arc column. Therefore, the radiometer viewed a section of the column that always included the entire arc diameter. As shown in Fig. 3, the section of the arc column viewed was halfway between the anode and cathode. Total radiation measurements were obtained in the wavelength range from 0.22 to 2.3 μ (the range of high transmittance for the fused silica tube).

Calibration

The radiometer was calibrated using a standard lamp (a General Electric DXW quartz-iodine tungsten filament lamp having known spectral characteristics). The 2.54-cm-long filament of the lamp was positioned in a location equivalent to the position of the centerline of the dc arc in Fig. 3, within the viewing field of the radiometer. The known intensity of radiation from the standard lamp at the location of the thermopile element was used to calibrate the radiometer. Two alternate methods for measuring the arc radiation were used in previous tests (Ref. 15)---one employed a blackened sleeve around the arc, and the other employed an annulus of water containing dye. Radiation measurements made by these two alternate methods

were consistent with the calibrated radiometer measurements made at that time. In addition, another method was used in the present study---absorption of radiation in a blackened copper slug (discussed in the section entitled SIMULATED PROPELLANT HEATING TESTS). The results also showed good agreement with the calibrated radiometer measurements.

Results

Results of measurements of the power radiated from the dc arc plasma in the modified configuration are summarized in Fig. 4. The results are expressed as the power radiated from a 12.7-cm test section -- the length of the test section used subsequently in propellant heating tests -- as a function of total arc power. Total power radiated in the test section length was obtained by multiplying the power radiated from a 2.54-cm arc length, as measured by the radiometer, by a factor of five. As shown in Fig. 4, the power radiated from the test section length ranged from 30 kW to 322 kW, while the corresponding total arc powers ranged from 110 kW to 780 kW. Thus, the maximum total arc power was increased above the levels in Ref. 14 from 480 kW to 780 kW, and the maximum power radiated from the 12.7-cm test length was increased from 238 kW to 322 kW. For these tests, it is estimated that the radiation efficiency, defined as the power radiated from the arc column per unit length divided by the power deposited in the arc column per unit length, ranged from 50 to 80 percent.

Figure 5 illustrates the operating characteristics of the dc arc. Figure 5(a) shows oscilloscope traces of the variations of anode-to-cathode voltage and arc current with time during a typical high power test. All dc arc operating data were obtained from traces similar to these. The arc voltage and current were relatively steady during the 0.5-sec tests, although, as shown in Fig. 5(a), the current trace showed pickup of ac noise. Current was determined by reading to the center of the noise. The variation of arc voltage with arc current is shown in Fig. 5(b). DC arc voltage ranged from 92 V to 183 V while dc arc current ranged from 1040 A to 4250 A. The maximum electrical power deposited in the arc column was about 34 kW/cm.

For all tests, the dc arc configuration, argon flow rate, inlet geometry, cathode position, and vortex flow injection angle were held constant. Test times for all tests were about 0.5 sec. The ballast resistance was varied to permit arc operation over the power range shown.

Increased dc arc power was obtained using the same equipment configuration as reported in Ref. 14. Current increases were obtained by operating the power supplies at an overload condition for these short test times. The steady state power supply rated current output is 2000 A, compared with 4250 A used in the tests.

Modifications to the arc vortex flow configuration were also required to permit operation at the increased current levels. Although the dc arc operated successfully in this configuration, there were clear indications that the configuration was reaching its limit of practical high power operation. For tests near the highest power, cracking of the fused silica tube frequently occurred from 1 to 30 min after the test was completed. Also, anode erosion occurred in some tests at the highest current levels. These difficulties present time-consuming inconveniences rather than absolute limitations. Efforts will be made to minimize their effects prior to the next test series.

COLD-FLOW TESTS

Objective

The major objective of the cold-flow tests was to develop a simulated propellant flow configuration which could subsequently be heated to high temperatures by absorption of thermal radiation. The desired flow configuration was similar to the propellant flow in the nuclear light bulb engine in the sense that (1) opacity of the central portion of the flow was provided by tungsten particle seeds and (2) buffer layers of unseeded gas separated the central flow from the duct walls, preventing possible coating of transparent duct walls. Use of tungsten seed necessitated cold-flow testing to determine an inlet and buffer flow configurations suitable for the simulated propellant heating tests. The flow requirements for tungsten seed were expected to be different from those for the carbon seed used in earlier tests (Refs. 14 through 16).

Flow System and Powder Feeder

Figure 6 is a schematic diagram of the simulated propellant flow system and high pressure (20 atm) rotating drum powder feeder system. These systems provide the required flows of tungsten seed, carrier, gas, and buffer gas. Tungsten powder having a nominal diameter of 0.35 μ was used to provide the opacity required for the simulated propellant heating tests. Tungsten was used for the simulated propellant seed because of its high melting and boiling points and because it is the propellant seed used in the reference nuclear light bulb engine.

Use of tungsten seed required the development of a new powder feeder to provide high tungsten powder flow rates (> 5 g/sec). Figure 6 illustrates the rotating drum powder feeder developed to meet these requirements. Rotation of the drum containing tungsten powder allowed an argon carrier flowing through the drum to entrain tungsten powder near the outlet of the drum. The tungsten-particle/argon aerosol then flowed to the seeded gas inlet of the simulated propellant flow system. Further details of the powder feeder configuration operating principles and performance characteristics are given in Appendix A. Also discussed in Appendix A are details of powder feeder operation with orifices for seed deagglomeration.

Two argon flow lines for the unseeded buffer layers were also connected to their respective inlets of the simulated propellant flow system. Individual pressure regulators, pressure guages, control valves, and flow metering equipment were used for each flow. Argon flow rates were measured using rotameters and variable area meters. After the simulated propellant flowed through the test section, the tungsten was removed before the argon exhausted to the atmosphere.

Figure 6 shows a sketch of a tungsten powder collecting chamber used for many of the tests. Collection was accomplished by gravitational settling of most of the powder. The remainder was collected in two 5.0-cm-thick fine pore filters. The chamber had a 30-cm i.d. and was about 1 m long.

Configuration

A cross section of the rectangular propellant duct mock-up is shown in Fig. 7. The simulated propellant duct was a separate assembly which could be attached to the inlet housing. Construction was such that the spacing between the two transparent fused silica walls was adjustable. These transparent walls extended beyond the 12.7-cm-long test section. The remaining two sidewalls of the simulated propellant duct mock-up were aluminum in the 12.7-cm test section; beyond the test section, the sidewalls were glass to allow observations of the buffer width as the simulated propellant left the test section. The aluminum side walls and their glass extensions were allowed to contact the seeded gas flow. These side walls became coated by the tungsten seeds.

The gas inlet shape shown in Fig. 7 is the same as that used for the tests reported in Ref. 14. The inlet passages are rectangular in cross-section for both buffer flows and the seeded flow. Porous foam was used in both buffer layer inlets to smooth the flow (see Fig. 7 for locations of the foam). Figure 7 also shows the locations of flow straighteners at the beginning of the test section. Various types of flow straighteners were tested. Several buffer width and flow relationships were also tested. The most promising results of these configuration changes were used to arrive at the final flow configuration.

Results

Tests with Carbon Seeds

Requirements for high seed weight flow rates cause conflicting requirements for the simulated propellant flow conditions. One requirement is to minimize velocity shear between the seeded gas and buffer flows. However, matching gas velocities at the inlet causes a large mismatch in the weight flow rates and fluid momentums between the seeded-gas flow and the buffer-gas flows. There have been studies of the effect of density differences on the mixing of parallel flowing streams; however, no studies have been found that treat flows with very large density ratios (> 10), such as are present in these tests. Another factor affecting the mixing is that the dense stream is composed of a particle flow; the solids may lag the gas and aggravate flow problems.

Qualitative cold-flow tests were made of the effects of velocity ratio, density ratio, and flow straightener configuration using carbon seed. Carbon seed was used because a comparison can be made with the results obtained in the tests discussed in Ref. 14. The configuration shown in Fig. 7 was used with two 1.5-cm-wide buffer inlets and a 0.3-cm-wide seed gas inlet. Seed inlet velocity ranged from 0.15 m/sec to 1.0 m/sec. Buffer-gas inlet velocities ranged from 0.5 m/sec to 7.0 m/sec. Carbon weight flows ranged from heavy to light (a heavy carbon flow corresponds to about 1.0 g/sec).

Good buffer layer performance was obtained at flow conditions similar to those reported in Ref. 14 (all velocities matched at 0.8 m/sec and a carbon weight flow less than about 0.5 g/sec). Best performance was obtained with 45 ppi foam across the inlet as a flow straightener. However, the porous foam cannot be used with the tungsten seed because it clogs rapidly.

Two honeycomb flow straightener configurations were also used. The first configuration consisted of two staggered layers of 1.27-cm-thick hexagonal cell honeycomb (0.32-cm nominal cell size); the second honeycomb configuration was a single piece of 2.54-cm-thick, 0.32-cm hexagonal cell honeycomb. The flow straighteners were located across the inlet as shown in Fig. 7. Tests were also conducted with no flow straightener at this location. The buffer layers were thinner for the honeycomb flow straightener configurations, and still thinner with no flow straightener. One-piece honeycomb appeared to give better results than the staggered configuration.

Increasing the buffer-gas velocity above the seed inlet velocity caused a slight increase in buffer layer thickness within the limits of the velocity ranges already described. Except for very light seed flow rates, when the buffer-gas velocity was less than the seed inlet velocity, the seed flow filled the duct, leaving no visible buffer layer. For all the conditions tested, heavy carbon flows caused the seeded portion of the flow to spread so that it reached the walls by the end of the test section. Increasing the carbon weight flow at any given flow condition was observed to cause a reduction in buffer layer thickness.

The results of these tests with carbon indicated that increased seed weight flow decreased the buffer layer thickness at a given flow condition and that decreased buffer gas flow also decreased the buffer layer thickness. However, below a critical buffer flow (flow dependent upon the seed flow rate), the seed flow filled the duct, coating all walls. The buffer layer thickness at any given flow condition was largest with porous foam flow straighteners, smaller with the two honeycomb flow straighteners, and smallest with no flow straightener. Based on these qualitative observations, it appears that there is a minimum buffer flow which must be provided for any given seed flow condition to prevent the seed from reaching the transparent propellant duct wall.

These observations helped provide an understanding of the flow requirements. However, further tests were required using tungsten seeds, since the anticipated tungsten flow rates were higher than the highest carbon flow rate that was used by a factor of about five.

Tests with Tungsten Seeds

Tests with Propellant Duct Mock-Up

Comparison of carbon and tungsten seed tests using the propellant duct mock-up (Fig. 7) indicated that steadiness of the tungsten flow was an important factor in obtaining satisfactory flow conditions. Steps were then taken in the powder feeder development to insure steady tungsten flow over the range of conditions expected to occur in the simulated propellant heating tests (see Appendix A for discussion of powder feeder steadiness).

A series of cold-flow tests was conducted using configurations similar to those used for the carbon tests, i.e., parallel duct walls, two 15-mm-wide buffer layer inlets, and a 3-mm-wide seeded gas inlet (see Fig. 7). Tungsten weight flow rates ranged from 5 g/sec to 15 g/sec. Orifices with 0.094-cm diam were used for seed deagglomeration. Seed inlet gas velocities ranged from 0.75 m/sec to 6.1 m/sec. Buffer-gas velocities were either matched with the seed-gas velocity, or ranged up to 15.3 m/sec. These test conditions were repeated with a honeycomb flow straightener in the test section inlet, and then with no flow straightener in the inlet. Qualitative observations were made of the buffer layer performance. It was observed that the buffer layer appeared to improve (contain less seed material) for higher buffer-gas velocities. Performance was better for the honeycomb configuration consisting of two staggered layers of 1.27-cm-thick hexagonal cell honeycomb (0.32-cm nominal cell size). However, this configuration was not suitable for propellant heating tests because the walls became coated with tungsten.

A second series of cold-flow tests was run in which the seeder was operated at pressures of about 12 atm with a 0.094-cm diam orifice at the end of a 15.24-cm-long tube. The orifice was positioned at the entrance to the seed flow duct. A 0.32-cm hexagonal cell honeycomb (2.54-cm thick) was used as a flow straightener. The test section and inlet were modified so that one buffer layer was 2.6-cm wide and the other was 1.5-cm wide. The seed inlet was 0.3 cm wide. The velocity in the seed inlet was 1.3 m/sec, while the buffer-gas flows had average velocities ranging from 1.3 m/sec to 5.2 m/sec. Tungsten weight flow at the conditions indicated was about 10 g/sec. Results of these tests indicated that better buffer layer performance was obtained with the 2.6-cm buffer layer than with the 1.5-cm buffer layer. An unseeded buffer layer about 0.8-cm wide was obtained at 5.2 m/sec buffer velocity with the 2.6-cm inlet, while little or no unseeded buffer layer

was observed with the 1.5-cm inlet. Wall coating on the 1.5-cm side was less severe than it had been in the earlier cold-flow tests with tungsten. For tests at lower buffer velocities (2.6 m/sec), the seed flow filled the duct for both buffer inlet sizes.

Tests with Propellant Heating Test Section

Cold-flow tests with the simulated propellant duct mock-up provided a basis for choosing a final simulated propellant heating configuration. When the propellant heating test section preliminary fabrication was completed, it was modified for a simulated flow configuration with a 1.7-cm-wide buffer inlet on the inner straight wall, a 1.5-cm-wide buffer inlet on the rear divergent wall (divergence angle of 6.25°) and a 0.3-cm-wide seeded gas inlet. This geometry was successfully tested with a 5.6 m/sec front buffer velocity, a 7.7 m/sec rear buffer velocity, and a 0.5 m/sec seed inlet velocity. A tungsten flow rate of 5 g/sec was used. An unseeded buffer layer about 0.8-cm wide was obtained on the front wall; it was about 1.0-cm wide on the rear wall. Simulated propellant heating tests using the dc arc were then initiated with this configuration.

SIMULATED PROPELLANT HEATING TESTS

Objectives

This portion of the program was directed toward obtaining simulated propellant bulk exit temperatures in excess of 4445°K (or 8000°R) by the absorption of thermal radiation. The simulated propellant flow was similar to that of the nuclear light bulb engine in the sense that thermal radiation was absorbed by micron-sized tungsten particle seed and that buffer layers of unseeded gas prevented coating of the propellant duct walls by the tungsten seed. Moreover, as in the engine, the simulated propellant duct had diverging walls; for some tests, it had a reflector on the rear wall. The model was also similar in geometry and size to a propellant duct that could be used in a Nuclear Furnace in-reactor test.

Long-term objectives of the simulated propellant heating tests are to obtain bulk exit temperatures approaching 6660°K, with tungsten seed, as required for the reference nuclear light bulb engine (Ref. 3). It is desirable to obtain simulated propellant temperatures high enough that all the primary physical phenomena expected in the engine propellant can be studied. For example, such effects as absorption of thermal radiation by tungsten vapor, transparent-wall coating, and heat transfer to the duct walls should be studied in detail for increased confidence in the full-scale engine design.

Test Configuration, Diagnostics and Procedures

Test Configuration

The results of the tests discussed in previous sections of this report were used to arrive at the test configuration for the simulated propellant heating tests. A photograph of the assembled equipment is shown in Fig. 8. The segmented mirror cavity focused thermal radiation from the dc arc on the simulated propellant flow. After being heated by absorption, the simulated propellant flowed into the water-cooled calorimeter used to determine bulk exit temperature. Tungsten powder was removed from the argon flow after the aerosol left the calorimeter by the powder-collecting chamber (Fig. 8). Some tungsten powder also collected in the calorimeter.

Figures 9 and 10 show cross-sections of the propellant heating configuration. Figure 9 is a cross-section of the lower portion. Section A-A shows the 4.0-cm-i.d. fused silica tube that enclosed the dc arc within the mirror cavity. Segmented fabrication of the mirror cavity allowed adjustment of the cavity shape, replacement of sections of the cavity if damaged, and repair of damaged sections. The fused silica tube was separated from the mirror surfaces by distances greater than 0.3 cm. Reflecting surfaces of the water-cooled copper mirrors were polished Kanigen (a trade name for a chemically-deposited nickel alloy coating), vapor-coated with aluminum.

The front and rear walls of the simulated propellant duct were 0.25-cm-thick uncooled fused silica plates (Fig. 9). Spacing between the fused silica plates was 3.5 cm at the test section inlet. The rear simulated propellant duct wall diverged from the front wall at an angle of about 6.25°, resulting in a spacing between the fused silica walls of 4.9 cm at the entrance to the calorimeter (Fig. 10). Both sides of the duct were made of uncooled copper. For most of the tests, a reflector was located behind the rear fused silica wall of the simulated propellant heating test section. As shown in Figs. 9 and 10, this reflector was made of two separate mirror segments which were the same size as the smaller of the arc mirror cavity segments.

As illustrated in Fig. 9, seeded gas was introduced into the central portion of the simulated propellant flow and was separated from the front and rear transparent walls by unseeded buffer layers. The seeded gas was allowed to contact the copper side walls. For all the tests, argon seeded with micron-sized tungsten particles was used as the simulated propellant. The simulated propellant entered the lower end of the 12.78-cm-long test section and flowed upward parallel to the axis of the dc arc into the calorimeter.

For all tests, the inner wall buffer layer inlet was 1.7 cm wide, the outer wall buffer layer inlet was 1.5 cm wide, and the seeded gas inlet was 0.3 cm wide. The seed flow spread while passing through the test section as illustrated in Figs. 9 and 10. Porous foam (45 ppi) was used in both buffer layer inlets to smooth the flow. No porous foam was used across the inlet to the test section as in earlier tests (Refs. 14, 15 and 16), because cold-flow tests indicated that the porous foam clogged with the tungsten seed.

As shown in Fig. 10, the simulated propellant flowed into the calorimeter at the end of the test section. Cold-flow tests indicated that the presence of the calorimeter at the exit did not adversely affect the simulated propellant flow in the test section.

Also as shown in Fig. 10, the anode for the dc arc was located about 3.8 cm above the mirror assembly. This positioning was used to minimize possible dc arc shorting through the copper mirror assembly. The fused silica tube enclosing the arc also extended beyond the mirror assembly.

Diagnostics

Calorimeter Measurements

The position of the water-cooled calorimeter assembly relative to the test section is shown in Fig. 10. Its purpose was to measure, based on the water-cooling temperature change, the energy contained in the hot simulated propellant flow.

Because of the 0.5-sec test time, the calorimeter did not come to thermal equilibrium with the simulated propellant flow. As a result, the simulated propellant bulk temperature was determined using a transient method. Simulated propellant was allowed to flow through the system while the difference between the calorimeter inlet and outlet water-cooling temperatures was monitored using a thermopile and a strip-chart recorder. Then the dc arc was turned on for about 0.5 sec. Energy was removed from the hot simulated propellant and stored in the metal parts of the calorimeter which were, in turn, cooled by the calorimeter water. The water-cooling temperature rise was monitored until the temperature difference between the inlet and outlet returned to its value before the dc arc was turned on.

Figure 11 is an example of a calorimeter water-cooling temperature rise trace for a high-power propellant heating test. The response time of the calorimeter is long compared with the simulated propellant heating test time of 0.5 sec. The water-cooling temperature rise was integrated and related through the water-cooling flow rate to the total energy deposited in the calorimeter. This total energy divided by the test time gives the average rate at which energy was deposited into the calorimeter during the test. The average rate of energy deposited was then related, through the simulated propellant mass flow rate and specific heat, to the simulated propellant bulk exit temperature. The bulk temperature determined in this way is a time-averaged temperature over the propellant heating test time. As shown in Fig. 10, a chromel/alumel thermocouple recorded the temperature of the simulated propellant as it left the calorimeter after being cooled down. This thermocouple temperature returned to its initial value in about 2.0 sec. The temperature rise as determined by the thermocouple was added directly to the time-averaged bulk exit temperature determined above. The exit thermocouple temperature rise was generally less than 1.0 percent of the time-averaged bulk exit temperature rise determined by the calorimeter.

As shown in Fig. 10, the calorimeter had water-cooled walls and water-cooled coils in the upper section. The lower portion, which served as an adaptor to the test section, did not have coils. The water-cooled walls of the adaptor section extended down into the mirror housing to the end of the test section. Water from the adaptor passed upward and cooled the walls of the upper section containing the coils. Each of the two coils was separately water-cooled. The water-cooling for the entire calorimeter originated from one inlet in which water temperature was measured. Water-cooling to each component could be varied separately. Water-cooling flows from all components were collected in a plenum at the top of the calorimeter and removed through one main exhaust. The plenum was designed to promote mixing between the flows. Water temperature was measured in the exhaust after leaving the plenum.

The calorimeter was prevented from contacting the mirror housing by insulating pieces of super-mica (Fig. 10). A super-mica heat shield prevented direct ratiation from the arc to the calorimeter in the region between the top of the mirror housing

and the anode. The entire calorimeter assembly was enclosed in fiberglass insulation and wrapped with asbestos tape. All the water-cooling inlet and exhaust hoses were also wrapped in insulation. An asbestos heat shield was positioned as shown in Fig. 10 to prevent the hot exhaust gases from the dc arc from contacting the calorimeter. Tests were conducted to determine the thermal insulation effectiveness by blocking the test section off from the dc arc and initiating the arc (see later discussion of Fig. 13). During these tests, the calorimeter absorbed a negligible amount of heat, demonstrating that it was effectively insulated from its surroundings. Some of the radiation from the dc arc, which passed through the test section, was absorbed by the calorimeter when the test section was not blocked off. Most of this radiation can be blocked from direct entry into the calorimeter if the simulated propellant transmission is low. This effect is discussed later.

Radiation Measurements

Measurements were made of the radiation transmitted through the simulated propellant as it flowed through the test section with the dc arc on. These measurements were compared with the radiation passing through the test section at the same dc arc conditions without seeds flowing. This comparison gave a measure of the fraction of the incident radiation that was transmitted through the simulated propellant. These measurements were made at a position 3.0 cm from the entrance to the calorimeter using a fiber optic probe and a photomultiplier detector. Figure 8 shows the location of the probe which viewed the test section through a space between the rear-mounted mirrors (Figs. 9 and 10).

Measurements were made of the effect of the mirror assembly on increasing the arc radiation in the direction of the test section, using the configurations shown in Figs. 12 and 13. A copper slug with blackened front surface was used to absorb the radiation from the dc arc. The copper slug was 12.7 cm long, 2.37 cm wide and 0.64 cm thick. The blackened face of the copper slug was positioned in the test section just behind the front fused silica wall, as shown in Figs. 12 and 13. A thermocouple was placed in a hole drilled from the back side of the copper slug to within 0.16 cm of the blackened front face. The thermocouple was located in the center of the front face of the copper slug.

The temperature rise of the copper slug was monitored when the dc arc was turned on. It was observed to increase rapidly when the arc was on, level off shortly after the arc was turned off, and then decrease slowly after remaining at a constant value for about 2 sec. The constant value of copper slug temperature was used, together with the slug density, specific heat and test time, to calculate the heat flux from the arc. Thermocouples were also located at the top and bottom of the copper slug. These thermocouples generally read between 92 and 98 percent of the value of the thermocouple in the center. Lower values at the ends are to be expected because the view factor from the arc to an element of the slug on the end is lower than the view factor to an element in the center.

Radiation flux incident on the test section was measured with the copper slug for tests without the mirror configuration (Fig. 12) and tests with the mirror configuration (Fig. 13). These tests were conducted at total arc powers up to about 100 kW to determine the mirror multiplication factor. The effect of the segmented mirror assembly is shown in Fig. 14 where the radiation flux incident on the test section with mirrors is the ordinate and the radiation flux incident on test section without mirrors, at the same dc arc total powers, is the abscissa. As indicated by the line in Fig. 14, the segmented mirror cavity increased the flux incident on the test section over that from the arc alone by a factor of about 2.2. This represents a significant increase over the corresponding factor of 1.4 obtained with the cylindrical mirror used for the tests reported in Ref. 14. This increased mirror factor was an important element in achievement of the principal objectives of the simulated propellant heating program.

Test Procedures

The test procedures are discussed in detail in Ref. 14. All required water flows were turned on and left on during each test series. Preparations for dc arc ignition were made (detailed dc arc test procedure was discussed in Ref. 14). All instrumentation was turned on, buffer-gas flows were turned on, and the seed flow started. Calorimeter, exhaust gas thermocouple and fiber optic probe readings were recorded on strip charts. After the 0.5 sec of dc arc operation, the seed and buffer flows were turned off. When the calorimeter had returned to its initial level, preparations were started for the next test.

Results

Table I lists the values of argon weight flow, tungsten weight flow, incident radiation, seed transmission, radiation absorption, calorimeter measurement, calorimeter correction factor, heat in the gas, and bulk exit temperature for all data points.

Tests with Reflector in Rear

Tests were conducted with reflectors located behind the rear propellant duct wall (Figs. 9 and 10) at dc arc powers up to 780 kW, with about 322 kW of radiation from the 12.7-cm-long section of the dc arc adjacent to the test section. Up to 67 kW of radiation were directed toward the test section. This represents an increase by a factor of two over the 34 kW obtained in earlier tests (Ref. 14). Near the highest dc arc powers, difficulties were encountered with cracking of the fused silica tube surrounding the dc arc after some tests. Increasing anode erosion was also noted as the maximum current was approached (4250 A). These difficulties represented time-consuming inconveniences. However, they did not represent a limit on the maximum temperatures obtained.

Tungsten flow rates of 5, 5.5 and 7 g/sec were used for these tests. Powder feeder operating conditions providing these flows were obtained using the calibration methods described in APPENDIX A. Tungsten flow rates of 5 and 5.5 g/sec were obtained using two orifices of 0.079-cm i.d. The flow rates for two orifices of this size differ from those presented in APPENDIX A because longer connecting tubing was required to connect the powder feeder to the test section for the simulated propellant heating tests. The orifices were located as shown in Fig. 9 in the seeded gas inlet. A 7-g/sec tungsten flow rate was obtained using a 15.24-cm-long, 0.165-cm-i.d. tube. A single tube was used for the 7-g/sec flow rate because the fixture used to split the tungsten flow for the two orifices clogged up frequently at this flow rate. Powder feeder operation at pressures between 17 and 20 atm was required to obtain these tungsten flow rates.

Several combinations of argon flow and seed flow were used in an effort to maximize the bulk exit temperature while minimizing transparent wall coating. The inlet configuration used was described earlier (Fig. 9). The average velocity of the seeded gas flow, at the entrance to the test section, was 0.5 m/sec during all tests. For several tests, a front-buffer-gas inlet velocity of 5.6 m/sec was used with a rear-buffer-gas inlet velocity of 7.7 m/sec. This resulted in a total argon flow rate of 8.8 g/sec. Tungsten flow rates of 5, 5.5 and 7 g/sec were used with these argon flows. Buffer layer thickness at the exit of the test section was observed to decrease for increasing tungsten flow rate. A minimum thickness of about 0.7 cm was observed. For these tests, no tungsten wall coating was observed on the simulated propellant duct transparent walls during simulator propellant heating tests.

Inlet velocity combinations of (1) 2.8 m/sec for the front buffer with 3.8 m/sec for the rear buffer (4.4 g/sec total argon flow) and (2) 1.4 m/sec for the front buffer with 1.9 m/sec for the rear buffer (2.2 g/sec total argon flow) were used with a tungsten flow of 7.0 g/sec. Buffer layer thickness decreased for decreasing argon flow. A minimum buffer thickness of about 0.4 cm was observed for the 4.4 g/sec total flow case, resulting in no visible wall coating during propellant heating tests. A buffer thickness of about 0.2 cm was observed for several of the tests with 2.2 g/sec total argon flow. However, at this flow condition buffer performance was erratic. For some tests, clean walls were obtained; coating occurred during other tests at nominally the same conditions. At this flow condition, tungsten was found to fall back from the calorimeter during some tests. This could have caused the inconsistent buffer behavior.

Simulated propellant heating data obtained when wall coating occurred were not used. When wall coating did occur, for most tests only the front wall was coated, while the rear wall remained clean. When the front wall coated, it appeared to be plated with tungsten which could not be removed except by repolishing the fused silica wall. This coating indicates that tungsten vapor and/or liquid were present in the flow as expected at the temperatures obtained.

Minimum buffer layer thickness and minimum argon flow maximizes the bulk exit temperature obtained at any given test condition. Therefore, further tests of optimum inlet buffer flow rate and tungsten flow rate are required for the determination of the flow condition with the smallest reliable buffer layer thickness and argon flow. Time limitations prevented further investigations of flow conditions during the present program. However, it has been shown that thin buffer layers can be maintained which prevent any visible evidence of transparent wall coating by the tungsten seed.

Figure 15 shows the variation of simulated propellant bulk exit temperature with radiation incident on the test section for tests with mirrors behind the rear wall and for the flow conditions described in the preceding paragraphs. The table at the top of Fig. 15 describes the symbol codes for various argon and tungsten flow conditions. As shown, a maximum bulk exit temperature of 4515°K was obtained. Seven data points were obtained in the neighborhood of the 4445°K bulk exit temperature objective. Highest temperatures were obtained for the smallest total argon weight flow (2.2 g/sec) with the largest tungsten weight flow (7 g/sec). The data show that tests at the same tungsten flow rate (7 g/sec) with increasing argon flow rates yield lower temperatures for the same incident radiation.

The highest temperature obtained in previous tests using carbon seed (3860°K; Ref. 14) is shown on Fig. 15 by the open triangle symbol. Maximum temperatures obtained during the tests reported herein are within the range of interest for low-power nuclear light bulb engines. A reference nuclear light bulb engine operating at the maximum bulk exit temperature obtained (4515°K) would have a vacuum specific impulse of 1360 sec. Temperatures obtained are well beyond the 3300 to 3700°K propellant temperatures expected in in-reactor tests in the Nuclear Furnace. Furthermore, local temperatures somewhat higher than the bulk temperature measured are expected to have existed in the test section. Therefore, it is likely that some portions of the simulated propellant flow contained tungsten vapor. As the reference engine bulk exit temperature (6660°K) is approached, tungsten vapor has to be the dominant source of opacity. Thus, obtaining simulated propellant temperatures at which significant amounts of tungsten vapor are present is an important long-term objective.

Also shown on Fig. 15 are calculated lines of constant T_E/T^*, i.e., the ratio of bulk exit temperature to equivalent blackbody radiating temperature of the dc arc. The latter temperature is based on the assumption that the incident radiation shown on the abscissa in Fig. 15 is supplied by a body radiating with an emissivity of 1.0 at the temperature T^*. It is significant that, at the higher powers, the measured bulk exit temperatures fall close to the $T_E/T^* = 1.0$ line (within about 5 percent). In the reference nuclear light bulb engine design, a value of $T_E/T^* = 0.8$ was assumed. Thus, the data suggest that temperatures higher than the design value of 6660°K might be attained in the engine for the same operating power level.

Figure 16 shows the same temperature data as in Fig. 15, but with nominal radiation absorbed by the simulated propellant as abscissa. Nominal radiation absorbed was calculated based on the attenuation measured by the fiber optic probe corrected for reflection back through the simulated propellant by the mirrors in the rear of the duct (Figs. 9 and 10). A 100-percent reflectivity was used in the estimate. The heat absorbed calculated in this way is not the heat which would be measured as enthalpy in the gas because much of the heat absorbed is lost again by re-radiation from the hot gas mixture. Power in the mixture of argon and tungsten is given by

$$Q_{GAS} = Q_{ABS} - Q_{LOST} \tag{1}$$

Q_{GAS} is measured directly calorimetrically, and Q_{ABS} is estimated as described above. However, there is no practical way to measure Q_{LOST}. As expected, plotting in this way shows the high and low temperature data as a more closely connected set of points, since temperatire is related more closely to energy absorbed than to incident energy.

A correction to the calorimeter measurement was made for direct dc arc radiation passing through the test section to the calorimeter. The correction procedure used is described in Ref. 14. For the tests reported herein, calorimeter correction resulted in reductions of the calorimeter power which ranged from 8 percent for heavy seeding to 53 percent for light seeding. Simulated propellant bulk exit temperature was determined from plots like Figs. 17 and 18, which show the calculated variation of bulk exit temperature for various argon and tungsten flow mixtures as a function of the power in the mixture. The corrected simulated propellant power content was used. These curves are based on calculations using the thermodynamic properties of argon and tungsten presented in the JANAF tables (Ref. 17).

Tests Without Reflector in Rear

Some initial tests at low dc arc powers were performed without a reflector in the rear of the propellant duct. This was done so that the flow could be observed, and so that data would be available for determining the effect on temperature of the rear mirror. These tests used a total argon flow rate of 8.8 g/sec. The front buffer inlet velocity was 5.6 m/sec, rear buffer inlet velocity 7.7 m/sec, and the seeded gas inlet velocity 0.5 m/sec. Two 0.079-cm-diam orifices were used with tungsten flow rates of 4, 5 and 5.5 g/sec. The orifice location is shown in Fig. 9. No coating of the transparent wall was observed to occur during these tests. Results of these tests are shown on Fig. 19. Comparison of these results for tests with mirrors show, as expected, that higher temperatures were obtained for similar conditions with mirrors in the rear. This comparison is best seen by studying the data summaries presented in Table I for the two types of tests.

Summary of Key Simulated Propellant Heating Results

Bulk exit temperatures up to 4515°K were obtained using argon seeded with submicron-sized tungsten particles as the simulated propellant. These bulk exit temperatures are in the range of interest for low-power nuclear light bulb engines and exceed the temperatures expected in small-scale in-reactor tests. They are at temperatures at which some tungsten vapor can be expected in the simulated propellant flow. They were obtained with a divergent simulated propellant duct which used unseeded buffer gas to prevent wall coating by the tungsten seed, and with a reflecting rear propellant duct wall to reduce radiation losses.

At higher temperatures, larger amounts of tungsten vapor will be present in the simulated propellant flow. Based on the present tests, it is expected that a bulk exit temperature of about 5200°K can be obtained for the next test series -- a temperature at which significant amounts of vapor should be present. This temperature increase should be obtainable by (1) modifying the arc configuration, (2) obtaining a small increase in arc power by operating at slightly higher current overload conditions, and (3) improving the mirror configuration. Further improvements in the flow geometry of the simulated propellant will also contribute to higher temperatures.

REFERENCES

1. McLafferty, G. H.: Investigation of Gaseous Nuclear Rocket Technology -- Summary Technical Report. United Aircraft Research Laboratories Report H-910093-46, prepared under Contract NASw-847, November 1969.

2. McLafferty, G. H.: Survey of Advanced Concepts in Nuclear Propulsion. J. Spacecraft Rockets, vol. 5, No. 10, October 1968, pp. 1121-1128.

3. McLafferty, G. H. and H. E. Bauer: Studies of Specific Nuclear Light Bulb and Open-Cycle Vortex Stabilized Gaseous Nuclear Rocket Engines. United Aircraft Research Laboratories Report F-910093-37, prepared under Contract NASw-847, September 1967. Also issued as NASA CR-1030.

4. Krascella, N. L.: Theoretical Investigation of the Absorption and Scattering Characteristics of Small Particles. United Aircraft Research Laboratories Report C-910092-1, prepared under Contract NASw-847, September 1964. Also issued as NASA CR-210.

5. Krascella, N. L.: Theoretical Investigation of the Absorptive Properties of Small Particles and Heavy-Atom Gases. United Aircraft Research Laboratories Report E-910092-7, prepared under Contract NASw-847, September 1965.

6. Marteney, P. J., N. L. Krascella and W. G. Burwell: Experimental Refractive Indices and Theoretical Small-Particle Spectral Properties of Selected Metals. United Aircraft Research Laboratories Report D-910092-6, prepared under Contract NASw-847, September 1965.

7. Marteney, P. J. and N. L. Krascella: Theoretical and Experimental Investigations of Spectral Opacities of Mixtures of Hydrogen and Diatomic Gases. Air Force Systems Command Report RTD-TDR-63-1102, prepared by United Aircraft Research Laboratories under Contract AF 04(611)-8189, November 1963.

8. Krascella, N. L.: Tables of the Composition, Opacity, and Thermodynamic Properties of Hydrogen at High Temperatures. United Aircraft Research Laboratories Report B-910168-1, prepared under Contract NAS3-3382, September 1963. Also issued as NASA SP-3005.

9. Lanzo, C. D. and R. G. Ragsdale: Experimental Determination of Spectral and Total Transmissivities of Clouds of Small Particles. NASA TN D-1405, 1962.

10. Lanzo, C. D. and R. G. Ragsdale: Heat Transfer to a Seeded Flowing Gas from an Arc Enclosed by a Quartz Tube. NASA TM X-52005, 1964.

REFERENCES
(cont'd)

11. Marteney, P. J.: Experimental Investigation of the Opacity of Small Particles. United Aircraft Research Laboratories Report C-911092-2, prepared under Contract NASw-847, September 1964. Also issued as NASA CR-211.

12. Williams, J. R., J. R. Clement, A. S. Shenoy and W. L. Partain: The Attenuation of Radiant Energy in Hot Seeded Hydrogen - An Experimental Study Related to the Gaseous Core Nuclear Rocket. Quarterly Status Report No. 2, NASA Research Grant NGR-11002-068, prepared by Georgia Institute of Technology, February 1969.

13. Mie, G.: Ann. Physik. Vol. 30, 1919.

14. Klein, J. F.: Experiments to Simulate Heating of the Propellant in a Nuclear Light Bulb Engine Using Thermal Radiation from a DC Arc Radiant Energy Source. United Aircraft Research Laboratories Report K-910900-8, prepared under Contract SNPC-70, September 1971. Also issued as NASA CR-123199.

15. Klein, J. F. and W. C. Roman: Results of Experiments to Simulate Radiant Heating of Propellant in a Nuclear Light Bulb Engine Using a DC Arc Radiant Energy Source. United Aircraft Research Laboratories Report J-910900-1, prepared under Contract SNPC-70, September 1970. Also issued as NASA CR-111099.

16. Roman, W. C., J. F. Klein and P. G. Vogt: Experimental Investigation to Simulate the Thermal Environment, Transparent Walls and Propellant Heating in a Nuclear Light Bulb Engine. United Aircraft Research Laboratories Report H-910091-19, prepared under Contract NASw-847, September 1969. Also issued as NASA CR-107048.

17. Stull, D. R., et al: JANAF Thermochemical Tables. The Dow Chemical Company, Midland, Michigan, 1964.

LIST OF SYMBOLS

A	Area, cm^2
$\dot{m}_A$	Argon flow rate, g/sec
$\dot{m}_W$	Tungsten flow rate, g/sec
M_W	Weight of tungsten, g
P_F	Pressure in rotating drum powder feeder, atm
q_{INC}	Incident radiant heat flux, kW/cm^2
Q_{ABS}	Nominal absorbed radiation, kW
Q_{GAS}	Power content of gas, kW
Q_{INC}	Total incident radiation on test section, kW
Q_{LOST}	Absorbed power lost from simulated propellant (primarily by re-radiation), kW
Q_R	Power radiated, kW
Q_T	Total arc power, kW
t	Time, sec
T_E	Time-average bulk exit temperature, °K
T_W	Calorimeter water-cooling temperature rise, °K
T^*	Equivalent blackbody radiating temperature corresponding to incident radiant flux, °K
η_T	Fraction of incident radiation transmitted through simulated propellant, dimensionless

APPENDIX A

HIGH-PRESSURE ROTATING DRUM POWDER FEEDER

Tungsten powder was used as the simulated propellant seed for the first time during the tests described in this report. Estimates of the tungsten flow rates required for these tests indicated that a powder feeder of larger capacity and larger powder feed rate than currently available was required. Based on an understanding of the needs of the simulated propellant heating program and previous experience in powder feeder development (Refs. 14, 15 and 16), a high-pressure rotating drum powder feeder was developed.

The powder feeder was designed to overcome the difficulties encountered in producing a flowing aerosol of tungsten particles. The powder and feed mechanism (Fig. 20(a)) is located inside the rotating drum, which has a 20.3-cm i.d. and is 61 cm long. A variable-speed drive motor is used to control the angular speed of the drum. As shown in Fig. 20(b), the drum is supported by bearings located near the end. The powder feeder continuously drops the tungsten in front of the gas outlet, allowing tungsten to be entrained by gas flowing toward the outlet. As shown in Fig. 20(b), the outlet was located on the axis of rotation of the drum in one end plate. The gas inlet is located in a similar manner in the other end. A series of vanes located inside a rotating drum drop the powder in front of the outlet. The primary vanes (see Fig. 20(a)) are shaped such that powder picked up by them slides forward and toward the outlet of the chamber as the drum rotates. When a vane has been rotated to the proper angular position, the powder slides off the vane and a portion is entrained in the gas flowing toward the outlet. The remainder falls to the bottom of the drum to be picked up by another vane. This allows a very dense powder suspension to be maintained at the gas outlet. Presence of a dense suspension near the outlet helps reduce pulsing of the flow and allows the gas to entrain as heavy a loading of solid particulates as it can support. By using this rotating drum configuration, the powder feed rate past the outlet need not be carefully controlled because gas flow and outlet geometry can be varied to control the rate of entrainment of solids by the gas. Those solids that are not entrained are made available again for entrainment when they are picked up again at the bottom of the drum.

Figure 20(c) is a photograph from the inlet end of the drum with both end plates removed, showing the location of the outlet at the far end and the ten primary vanes. Primary vanes occupy the 12.7 cm nearest the outlet. Figure 21 is a sketch of one primary vane; there are ten such vanes. Each one is slanted at an angle of 25° to the axis of the drum and aimed toward the outlet as shown in Fig. 20. Secondary vanes, which feed powder forward to the primary vanes, are located in the rear of the drum. Secondary vanes are flat plates about 5.0 cm high and 12.7 cm long. They are slanted at an angle of 25° to the axis of the rotating drum. As

shown in Fig. 20(c), there are four stages of secondary vanes with one vane per stage. Each secondary vane stage occupies about 11.4 cm of the axial length of the drum. An internal screw is formed by these vanes which causes the powder to be fed forward, toward the primary vanes and the outlet.

Tests with the powder feeder were performed at pressures up to 19 atm. Tungsten flow rates between 4.0 g/sec and 27 g/sec have been obtained. Tests of various size orifices were conducted in which the seed flow rate was measured as a function of orifice pressure. For all the tests, an argon carrier flow rate of about 0.15 g/sec was used. Tungsten flow rate was determined by collecting the tungsten in a collecting chamber and measuring the weight change over a 30-sec test period. Figures 6 and 8 show the powder-collecting chamber as it was used for other portions of the program. The pressure in the drum was measured using a pressure gauge located as shown in Fig. 6. During some of the tests the back pressure decreased. At most, the decrease in pressure was about 5 percent of the drum pressure. Results of these tests are summarized on Fig. 22, which shows the variation of average tungsten weight flow rate with average pressure for orifices with diameters of 0.079 cm, 0.139 cm and 0.198 cm. As expected, larger orifices yield larger flow rates at a given back pressure. Data for a given size orifice are well-behaved and fairly repeatable. One might expect that the weight flow per unit area should be a function of back pressure. Figure 23 shows that a correlation exists between back pressure and weight flow per unit area over a range of 2 atm to 19 atm.

It was observed that the amount of tungsten present in the powder feeder affected the weight flow rate results. Figure 24 shows the variation of tungsten weight flow with the amount of tungsten remaining in the powder feeder after the test. The data shown are for tests using a 0.139-cm-diam orifice and a pressure in the feeder of about 13 atm. As shown, when less than 4 kg remained in the powder feeder, the weight flow showed a decrease with decreasing charge. Test conditions for data on Figs. 22 and 23 were chosen such that this effect was not present.

All the tests discussed above were performed using new tungsten powder. An effort was made to collect the powder for reuse because it is expensive. However, modified powder feeder operation was required to obtain steady tungsten flow rate when the tungsten was reused. Placing a baffle inside the rotating drum (Fig. 20(c)), and inclining the drum (see Fig. 6), smoothed the flow rate. Results of tests with the baffle and inclined drum are shown in Fig. 25. The results are similar to those shown on Fig. 23. Therefore, although the baffle and inclined drum helped smooth the flow, they did not cause significant variation of the powder feeder operating characteristics. Caution should be exercised in using the data shown in these figures because no attempt has been made to investigate its generality. These data represent operating characteristics for this feeder configuration under the operating conditions described.

It is currently expected that the principle of operation of the rotating drum powder feeder could be extended to higher pressures, other powder feed flow rate ranges, and other powder materials.

TABLE I

SUMMARY OF SIMULATED PROPELLANT HEATING DATA

Argon Weight Flow $\dot{m}_A$-g/sec	Tungsten Weight Flow $\dot{m}_W$-g/sec	Incident Radiation Q_{INC}-kW	Fraction of Radiation Transmitted η_T	Absorbed Radiation Q_{ABS}-kW	Calorimeter Power Q_{CAL}-kW	Calorimeter Power Correction Factor K	Power in Gas Q_{GAS}-kW	Bulk Exit Temperature T_E-°K
With Reflector in Rear of Propellant Duct								
2.2	7.0	68.27	0.04	65.54	14.84	0.91	13.56	4463
2.2	7.0	60.77	0.01	59.90	13.27	0.92	12.21	4298
2.2	7.0	64.50	0.02	63.24	14.13	0.92	12.99	4392
2.2	7.0	64.20	0.01	63.28	13.43	0.92	12.30	4299
2.2	7.0	67.90	0.03	65.19	15.11	0.92	13.92	4515
2.2	7.0	61.60	0.02	60.56	14.51	0.93	13.45	4441
2.2	7.0	44.08	0.03	42.65	10.61	0.93	9.82	3912
2.2	7.0	35.09	0.03	33.95	7.70	0.92	7.06	3468
2.2	7.0	54.44	0.03	52.68	9.23	0.89	8.17	3703
2.2	7.0	60.78	0.03	58.81	12.00	0.91	10.86	4069
2.2	7.0	63.00	0.03	60.96	14.20	0.92	13.05	4401
4.4	7.0	67.64	0.06	63.41	11.63	0.88	10.21	3475
8.8	7.0	67.21	0.12	58.98	16.22	0.91	14.69	3100
8.8	5.5	28.53	0.38	17.78	6.22	0.83	5.17	1389
8.8	5.5	28.53	0.33	19.23	6.39	0.85	5.42	1439
8.8	5.5	35.93	0.50	18.02	8.00	0.81	6.44	1639
8.8	5.5	37.52	0.50	19.19	9.08	0.83	7.49	1850
8.8	5.5	39.31	0.41	23.21	8.79	0.83	7.28	1822
8.8	5.5	39.63	0.46	21.31	8.43	0.81	6.79	1700
8.8	5.5	43.54	0.52	20.97	8.78	0.78	6.83	1733
8.8	5.5	43.43	0.49	22.15	8.50	0.78	6.61	1567
8.8	5.0	11.31	0.45	6.19	2.01	0.77	1.53	583
8.8	5.0	11.41	0.42	6.59	2.61	0.83	2.17	678
8.8	5.0	11.10	0.46	6.01	2.18	0.79	1.72	639
8.8	5.0	14.90	0.11	13.25	2.63	0.87	2.28	695

(continued)

TABLE I (cont'd)

SUMMARY OF SIMULATED PROPELLANT HEATING DATA

Argon Weight Flow $\dot{m}_A$-g/sec	Tungsten Weight Flow $\dot{m}_W$-g/sec	Incident Radiation Q_{INC}-kW	Fraction of Radiation Transmitted η_T	Absorbed Radiation Q_{ABS}-kW	Calorimeter Power Q_{CAL}-kW	Calorimeter Power Correction Factor K	Power in Gas Q_{GAS}-kW	Bulk Exit Temperature T_E-°K
With Reflector in Rear of Propellant Duct								
8.8	5.0	34.13	0.62	12.94	6.20	0.72	4.47	1111
8.8	5.0	38.36	0.35	24.96	7.02	0.80	5.63	1300
8.8	5.0	40.69	0.70	12.05	6.60	0.66	4.34	1061
8.8	5.0	40.69	0.77	9.39	8.77	0.73	6.41	1445
8.8	5.0	8.45	0.34	5.57	2.34	0.88	2.05	722
8.8	5.0	8.24	0.43	4.66	2.01	0.84	1.68	628
8.8	5.0	8.45	0.21	6.69	1.52	0.84	1.28	555
8.8	5.0	9.51	0.39	5.84	2.07	0.83	1.72	639
8.8	5.0	8.14	0.35	5.30	2.11	0.87	1.83	645
Without Reflector in Rear of Propellant Duct								
8.8	5.5	8.88	0.79	3.38	2.12	0.79	1.68	650
8.8	5.5	8.88	0.47	0.97	1.12	0.47	0.53	396
8.8	5.5	9.72	0.81	3.31	2.64	0.81	2.14	745
8.8	5.5	9.41	0.80	4.65	2.05	0.80	1.63	639
8.8	5.5	9.41	0.75	3.50	1.93	0.75	1.45	600
8.8	5.0	8.14	0.68	2.61	1.70	0.75	1.27	562
8.8	5.0	8.03	0.74	2.08	1.66	0.73	1.21	549
8.8	5.0	8.14	0.50	4.04	1.72	0.79	1.36	583
8.8	5.0	8.03	0.55	3.66	1.79	0.79	1.42	596
8.8	5.0	8.98	0.64	3.22	1.69	0.73	1.23	551
8.8	5.0	9.51	0.69	2.97	1.87	0.73	1.35	581
8.8	4.0	7.29	0.63	2.73	1.24	0.70	0.87	482
8.8	4.0	7.93	0.67	2.66	1.56	0.73	1.14	545
8.8	4.0	8.14	0.62	3.07	1.70	0.76	1.29	578

(continued)

TABLE I (Concluded)

SUMMARY OF SIMULATED PROPELLANT HEATING DATA

Argon Weight Flow $\dot{m}_A$-g/sec	Tungsten Weight Flow $\dot{m}_W$-g/sec	Incident Radiation Q_{INC}-kW	Fraction of Radiation Transmitted η_T	Absorbed Absorbed Radiation Q_{ABS}-kW	Calorimeter Power Q_{CAL}-kW	Calorimeter Power Correction Factor K	Power in Gas Q_{GAS}-kW	Bulk Exit Temperature T_E-°K
Without Reflector in Rear of Propellant Duct								
8.8	4.0	8.14	0.71	2.38	1.15	0.60	0.70	443
8.8	4.0	5.81	0.54	2.66	1.23	0.78	0.96	504
8.8	4.0	5.81	0.61	2.27	1.38	0.80	1.10	536
8.8	4.0	6.87	0.75	1.70	1.37	0.73	0.98	507
8.8	4.0	3.49	0.64	1.25	0.73	0.76	0.55	408
8.8	4.0	3.49	0.62	1.32	0.52	0.65	0.34	360
8.8	4.0	3.80	0.76	0.93	1.15	0.82	0.94	499
8.8	4.0	3.80	0.86	0.54	1.14	0.80	0.91	490
8.8	4.0	3.70	0.57	1.59	0.87	0.80	0.70	443
8.8	4.0	3.49	0.87	0.44	0.77	0.71	0.55	408
8.8	4.0	4.44	0.82	0.80	1.02	0.74	0.75	456
8.8	4.0	4.23	0.72	1.18	1.37	0.84	1.14	545
8.8	4.0	4.33	0.69	1.35	1.00	0.77	0.77	457
8.8	4.0	4.97	0.79	1.05	0.92	0.68	0.62	425
8.8	4.0	4.44	0.57	1.92	0.65	0.67	0.44	383
8.8	4.0	4.86	0.65	1.69	0.64	0.60	0.38	368
8.8	4.0	5.39	0.50	2.70	0.86	0.72	0.62	425
8.8	4.0	5.50	0.55	2.49	0.57	0.54	0.31	350
8.8	4.0	6.66	0.66	2.25	0.91	0.61	0.55	408
8.8	4.0	6.34	0.61	2.49	1.09	0.71	0.77	459
8.8	4.0	6.34	0.58	2.66	1.10	0.72	0.80	466

NUCLEAR LIGHT BULB CONCEPT AND DC ARC CONFIGURATION

SECTIONS SHOWN ARE AT AXIAL MID-STATIONS OF ENGINE UNIT CAVITY AND ARC EXPERIMENT

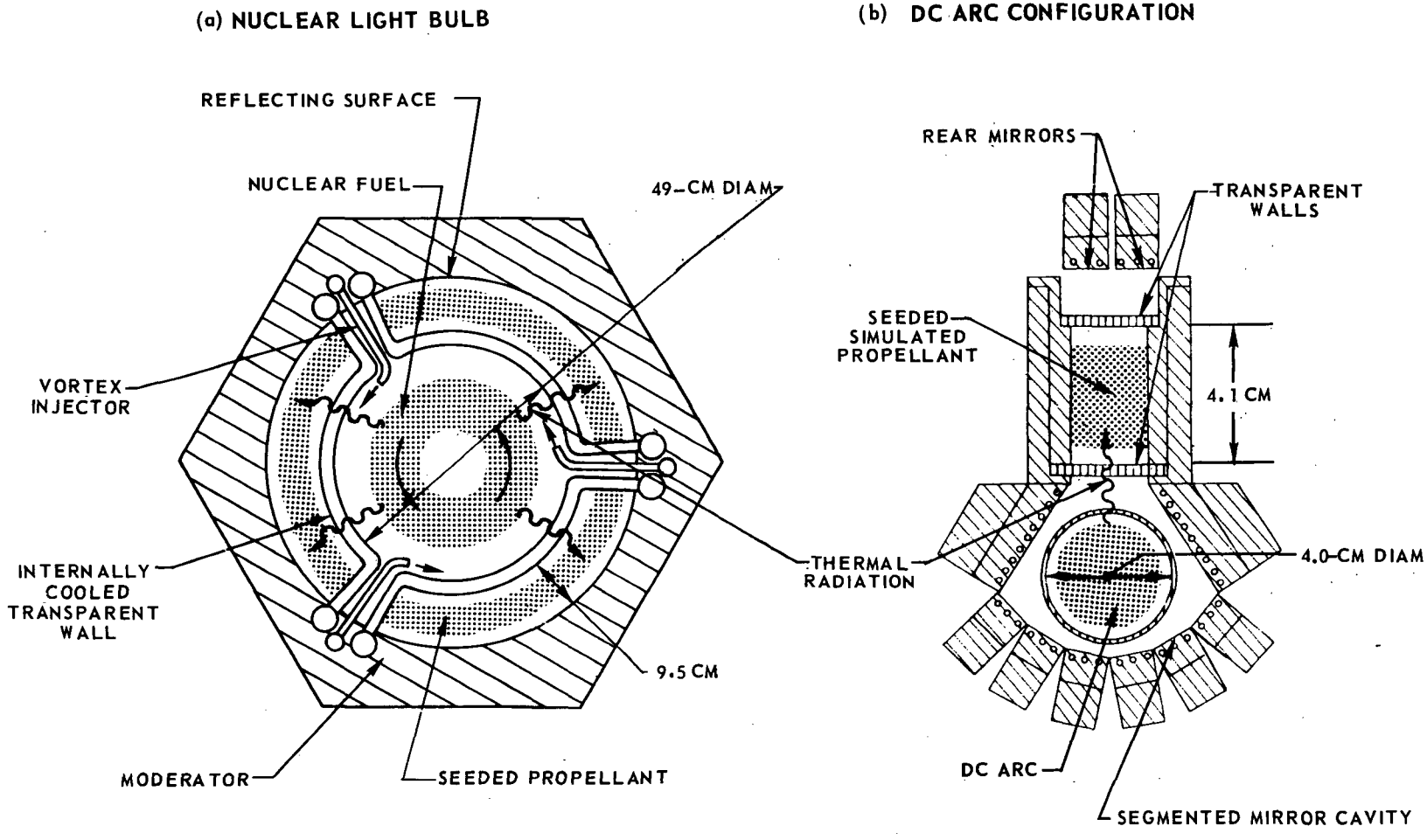

L-910900-13

FIG. 1

FIG. 2

DIMENSIONS OF UNIT CAVITY IN REFERENCE ENGINE

COMPLETE ENGINE IS COMPOSED OF A SEVEN-UNIT-CAVITY CLUSTER

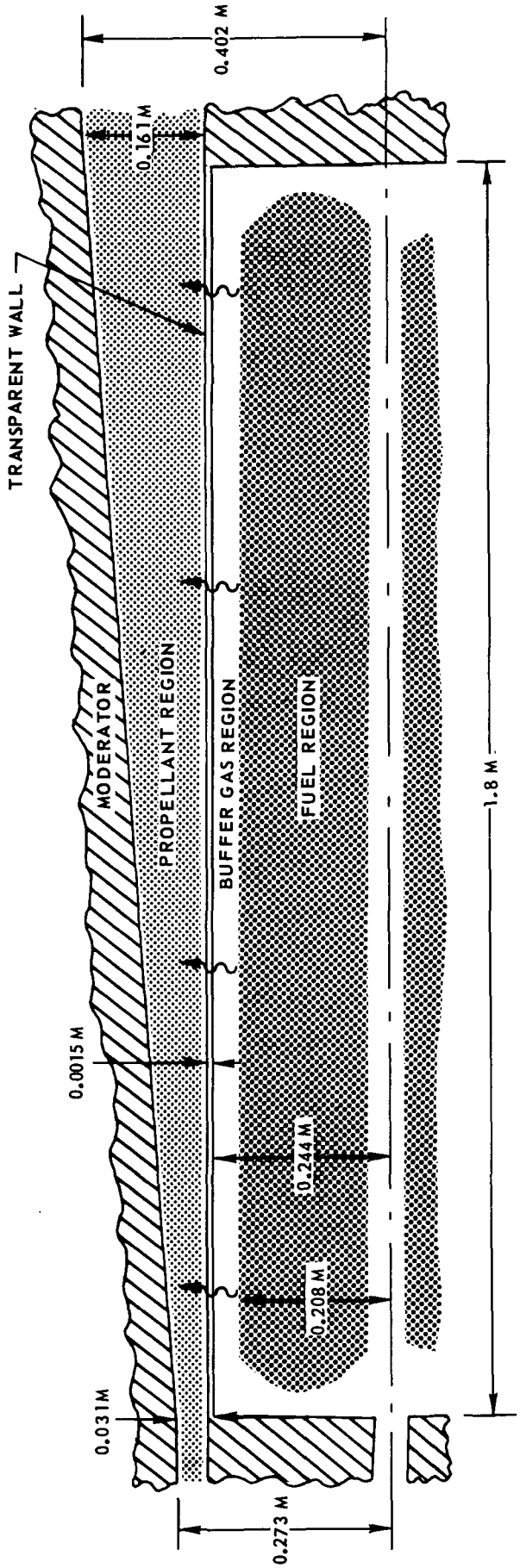

FIG. 3

SKETCH OF BASIC DC ARC AND RADIOMETER OPTICAL SYSTEM

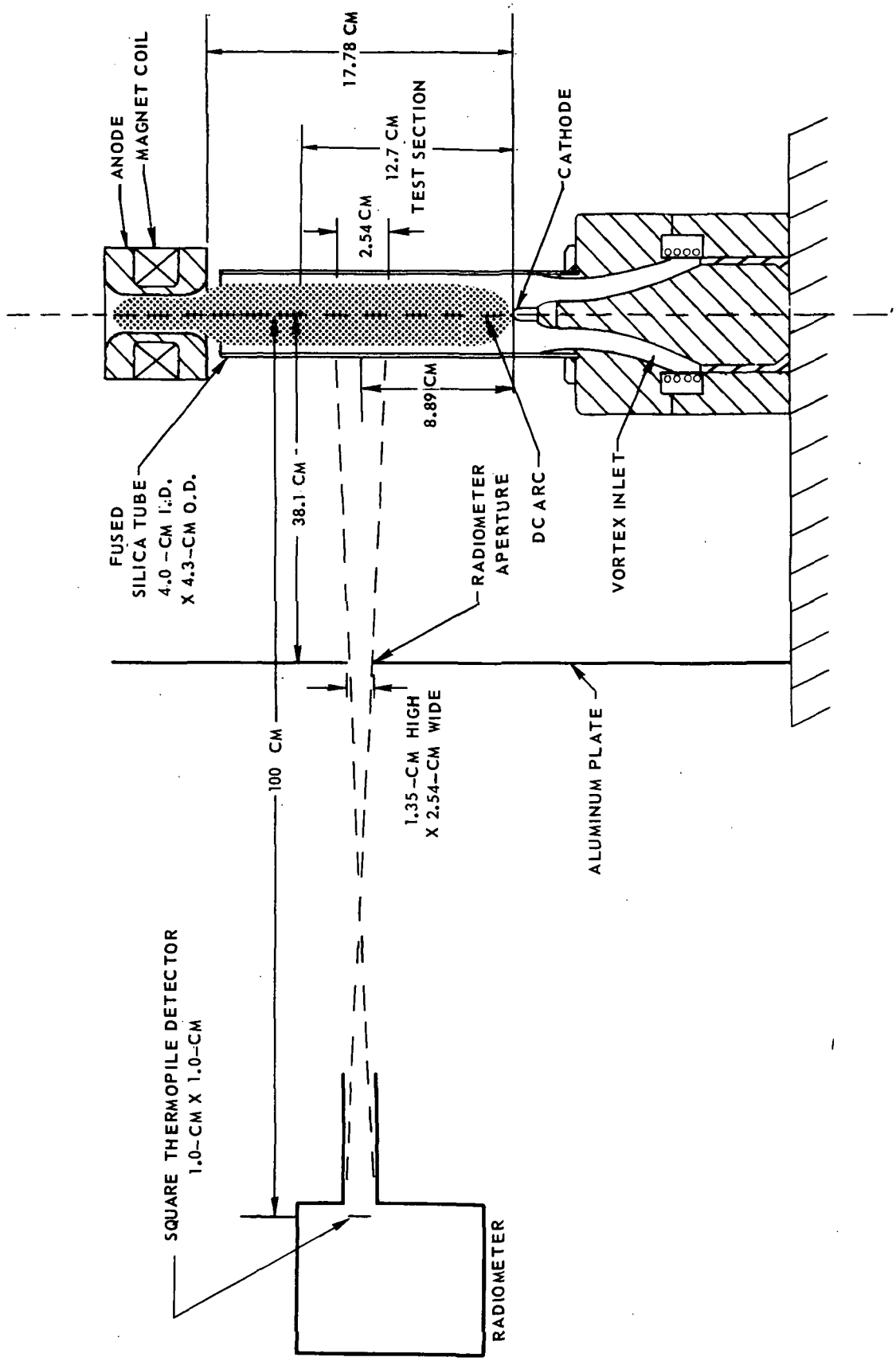

VARIATION OF POWER RADIATED FROM 12.7-CM TEST SECTION LENGTH WITH TOTAL ARC POWER

SEE FIG. 3 FOR ARC CONFIGURATION
1 ATM PRESSURE ARGON ARC
CATHODE TO ANODE DISTANCE = 17.78 CM
TEST TIME APPROXIMATELY 0.5 SEC
RADIATION EFFICIENCY PER UNIT LENGTH = 50 TO 80 PERCENT (SEE TEXT)

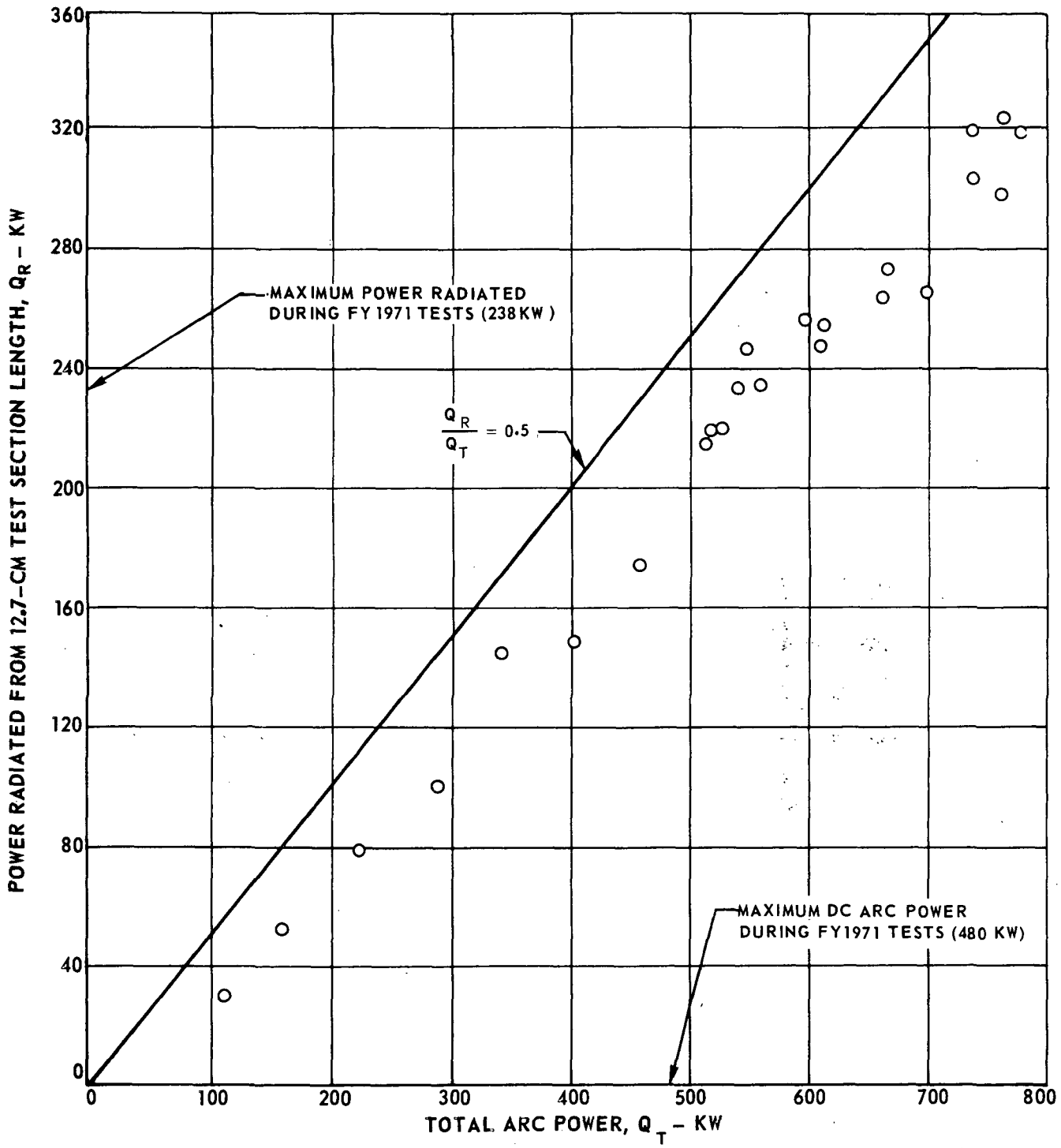

ELECTRICAL OPERATING CHARACTERISTICS OF DC ARC FOR PROPELLANT HEATING TESTS

SEE FIG. 3 FOR ARC CONFIGURATION
1 ATM PRESSURE ARGON ARC
CATHODE TO ANODE DISTANCE = 17.78 CM
TEST TIME APPROXIMATELY 0.5 SEC

a) VARIATION OF DC ARC VOLTAGE AND CURRENT WITH TIME FOR A TYPICAL TEST

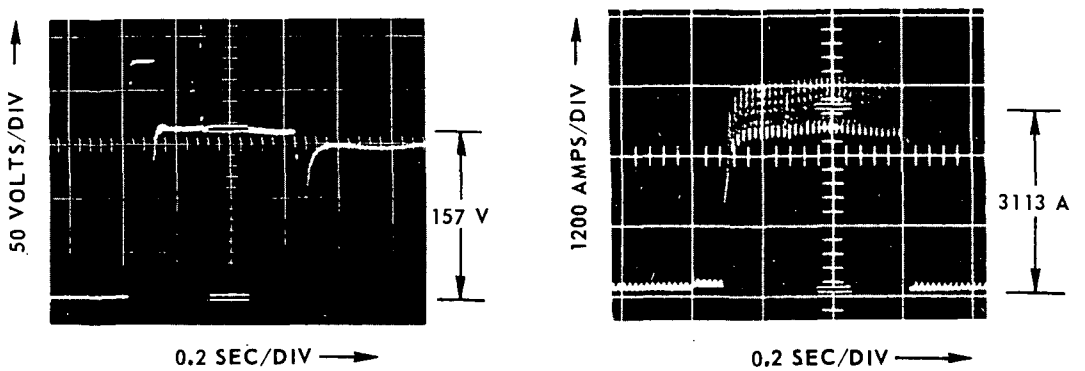

b) VARIATION OF DC ARC VOLTAGE WITH CURRENT

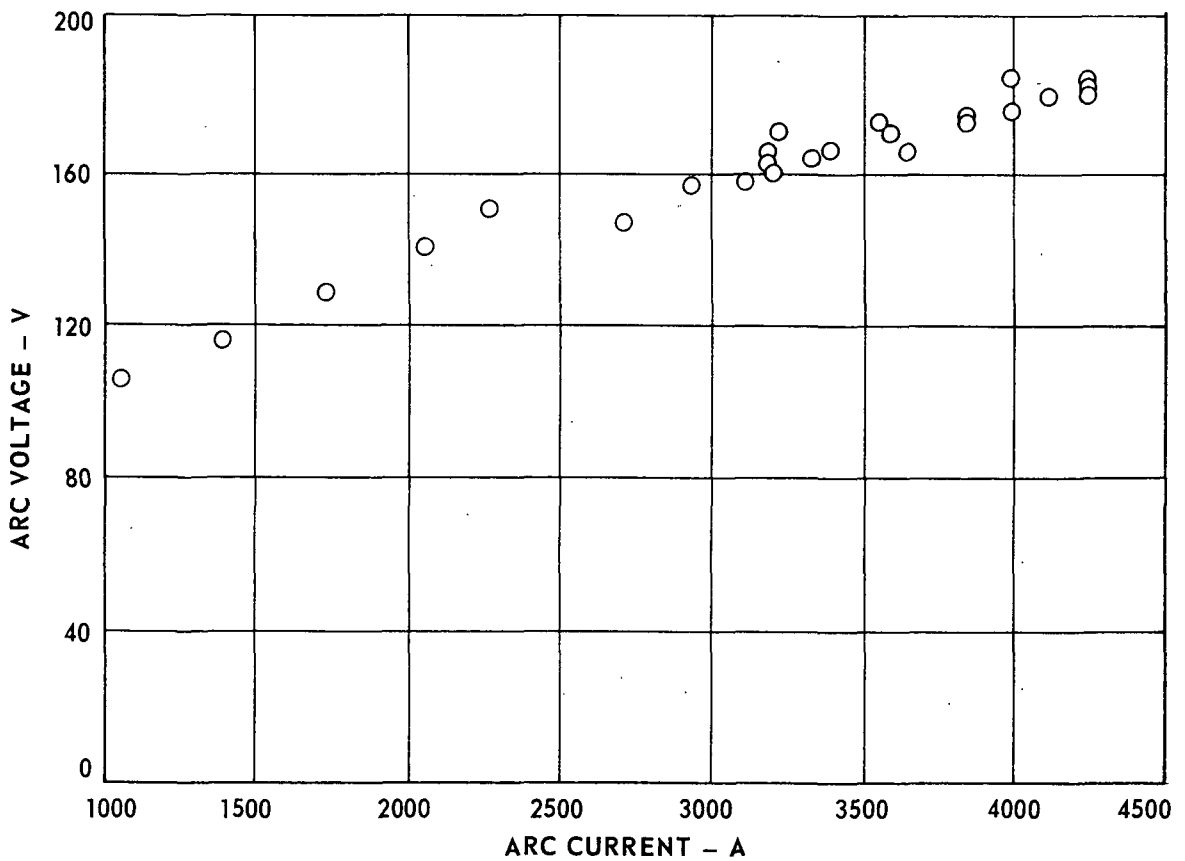

SCHEMATIC DIAGRAM OF SIMULATED-PROPELLANT FLOW SYSTEM AND HIGH PRESSURE ROTATING DRUM POWDER FEEDER SYSTEM

NOT TO SCALE

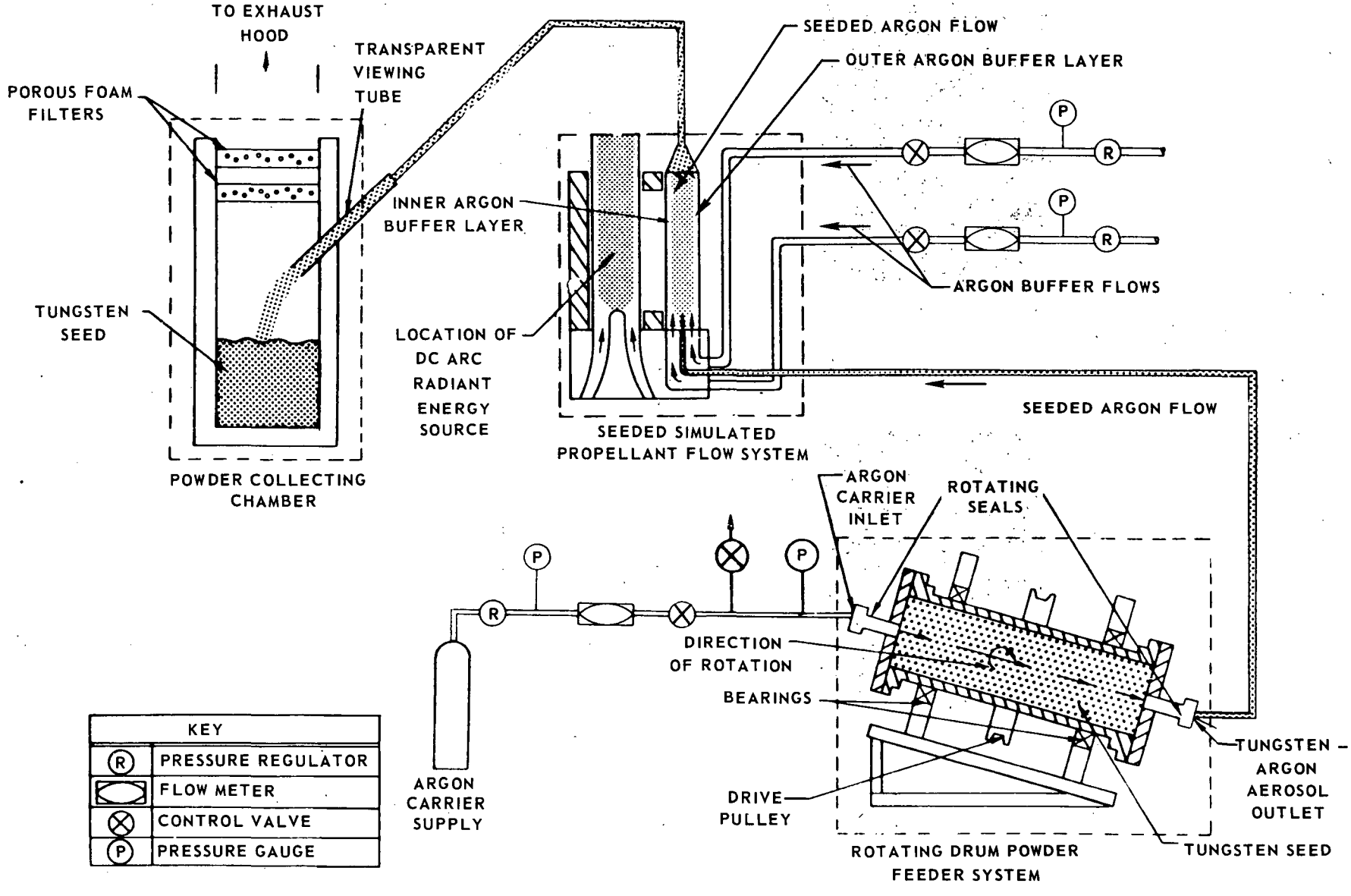

L-910900-13

FIG. 6

SKETCH OF CROSS-SECTION OF RECTANGULAR PROPELLANT DUCT MOCK-UP

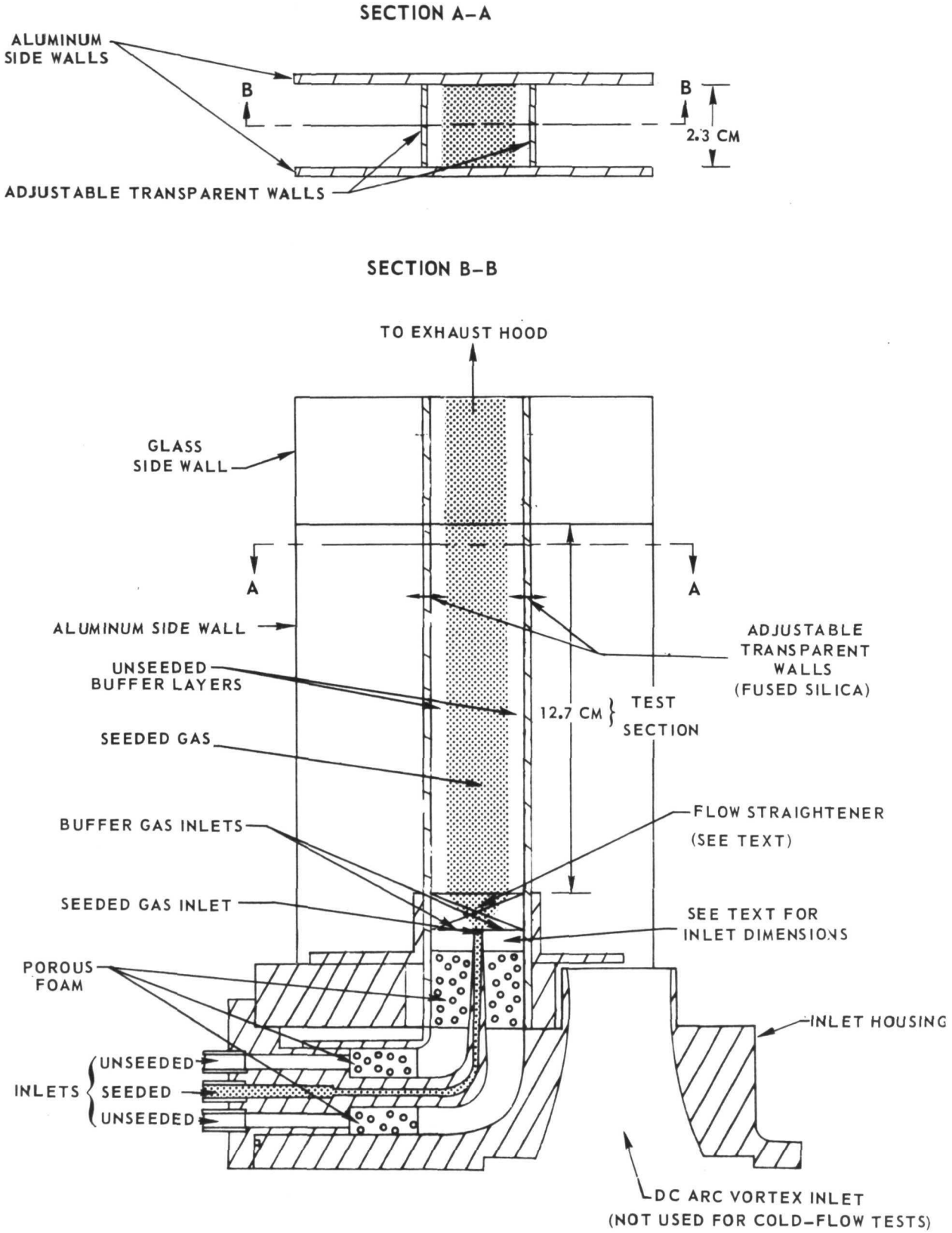

PHOTOGRAPH OF PROPELLANT HEATING EQUIPMENT

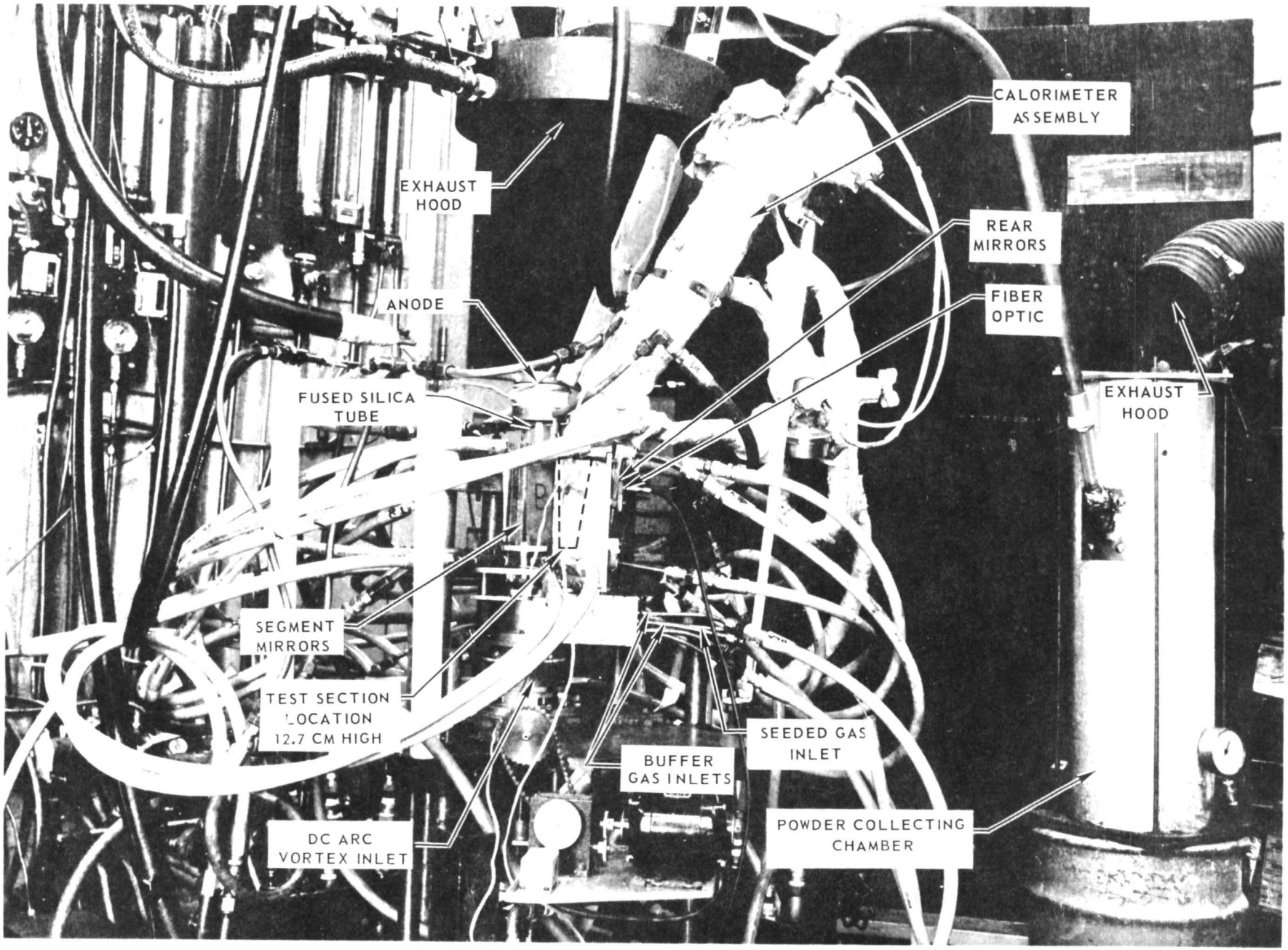

L-910900-13

FIG. 8

L-910900-13

FIG. 9

SKETCH OF LOWER PORTION OF PROPELLANT HEATING CONFIGURATION FOR TESTS WITH REFLECTOR IN REAR OF PROPELLANT DUCT

SEE FIG. 10 FOR UPPER PORTION DETAILS

SECTION A-A

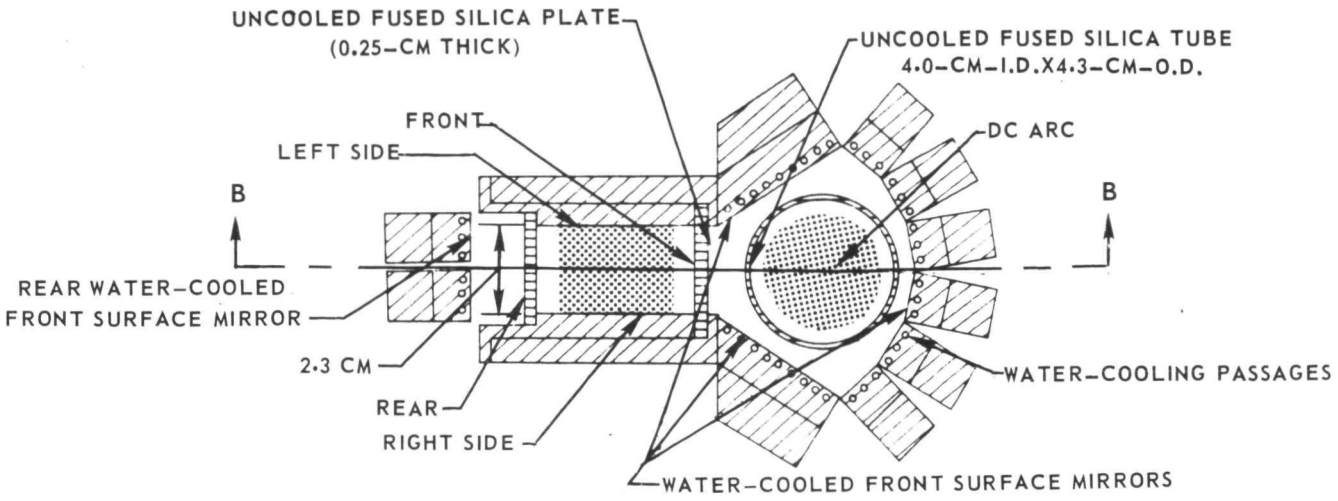

SECTION B-B

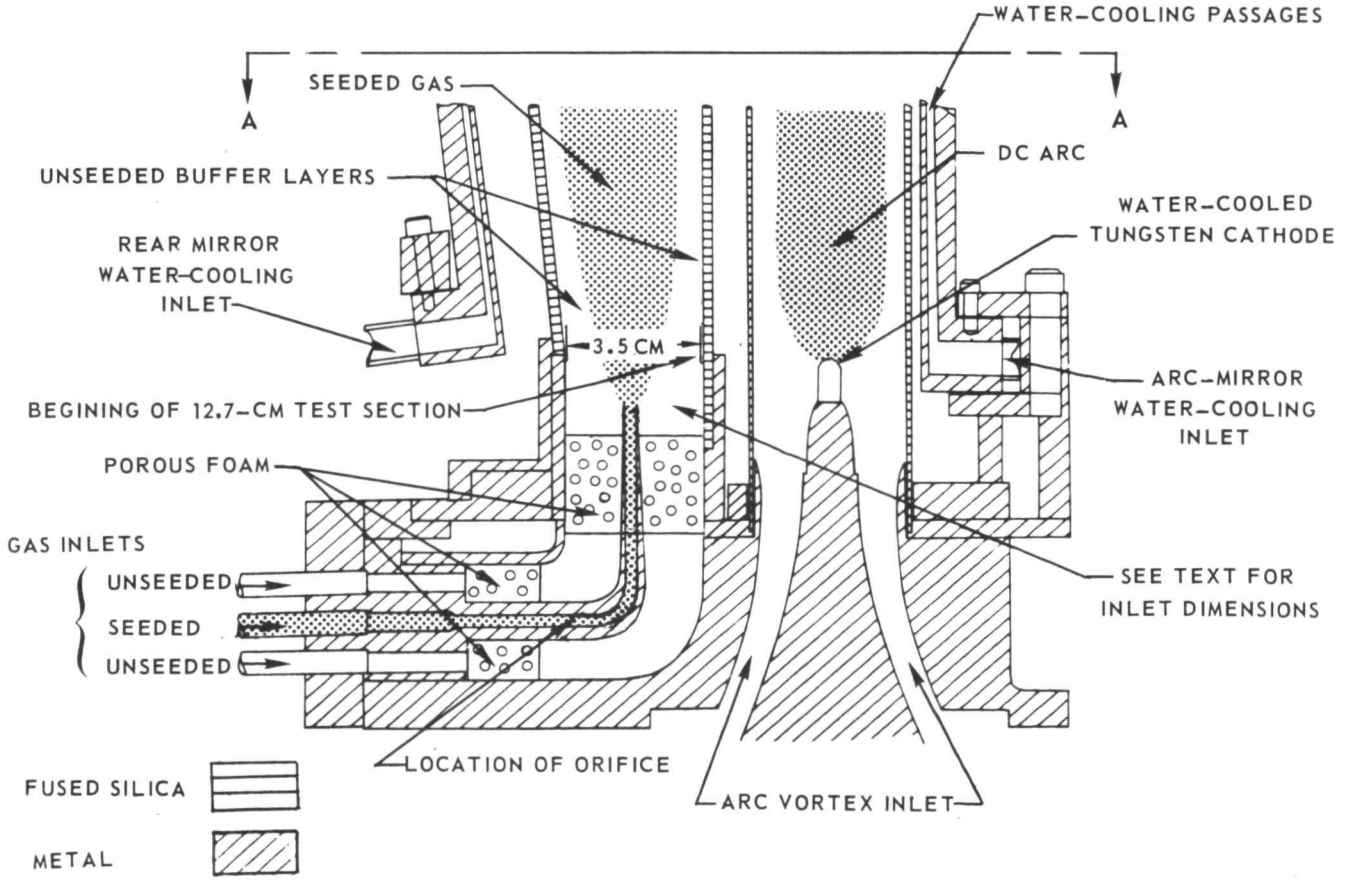

FIG 10

SKETCH OF UPPER PORTION OF PROPELLANT HEATING CONFIGURATION FOR TESTS WITH REFLECTOR IN REAR OF PROPELLANT DUCT

SEE FIG. 9 FOR LOWER PORTION DETAILS

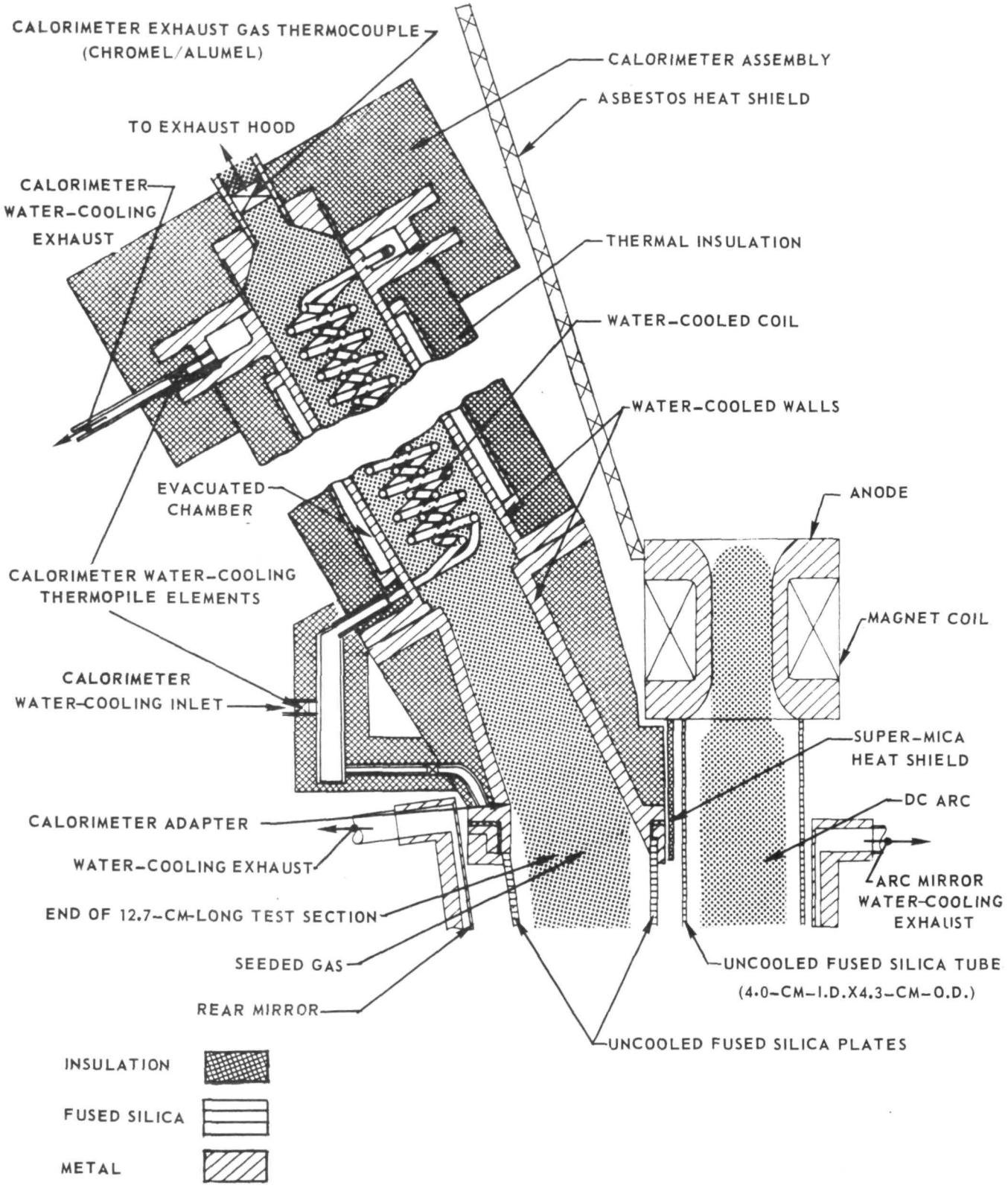

EXAMPLE OF CALORIMETER WATER-COOLING TEMPERATURE RISE TRACE

TEST CONDITIONS: ARGON FLOW RATE, $\dot{m}_A = 2.2$ G/SEC

TUNGSTEN FLOW RATE, $\dot{m}_W = 7.0$ G/SEC

BULK EXIT TEMPERATURE, $T_E = 4515$ °K

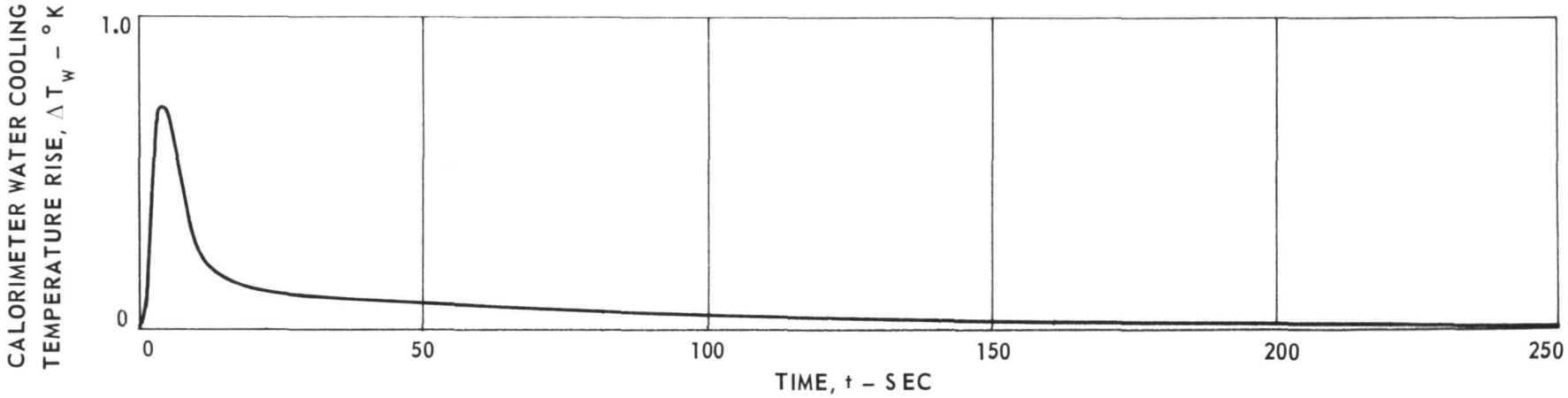

FIG. 11

FIG. 12

SKETCH OF DC ARC CONFIGURATION WITHOUT MIRRORS FOR COPPER SLUG RADIATION MEASUREMENTS

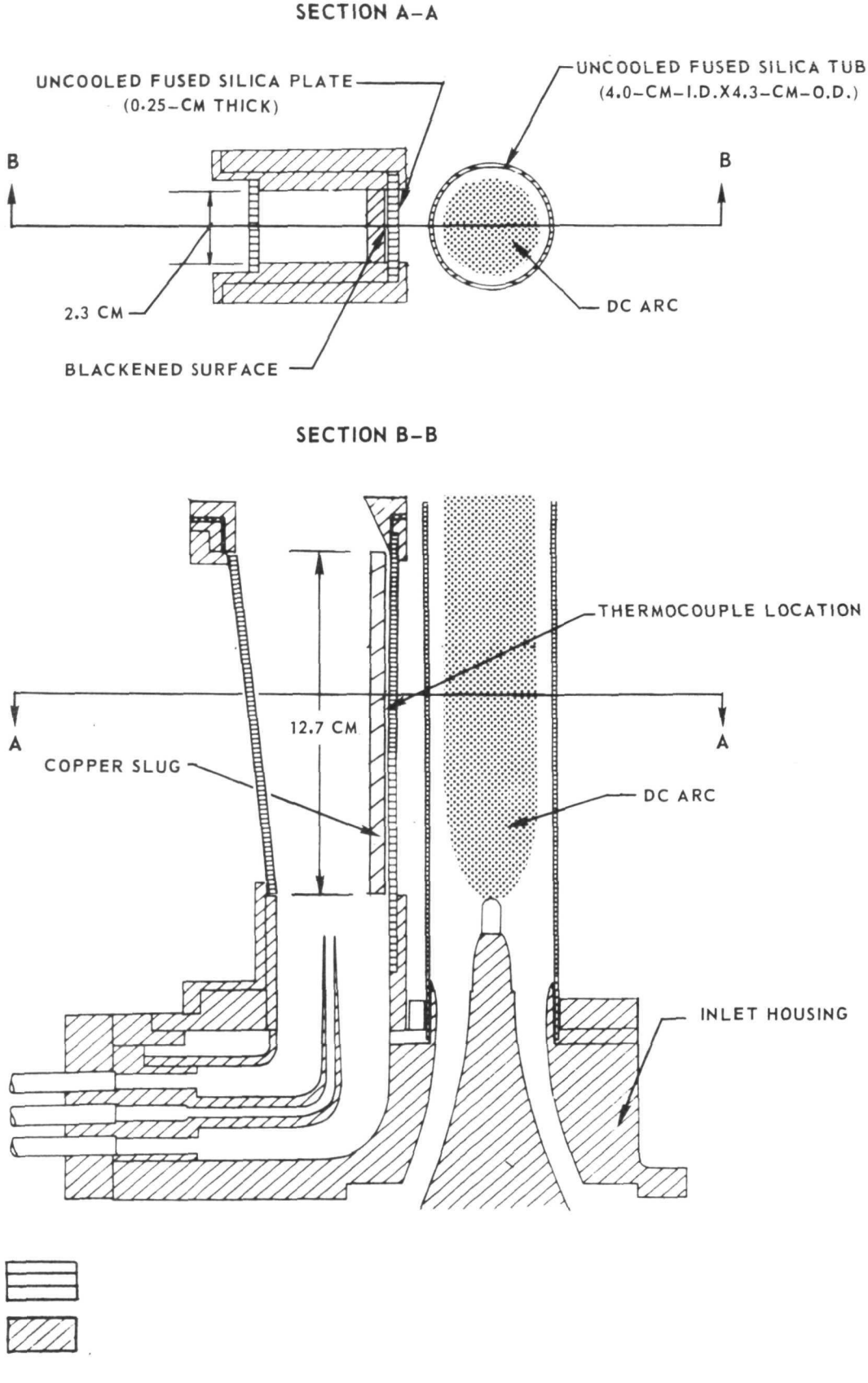

FIG. 13

SKETCH OF DC ARC CONFIGURATION WITH MIRRORS FOR COPPER SLUG RADIATION MEASUREMENTS

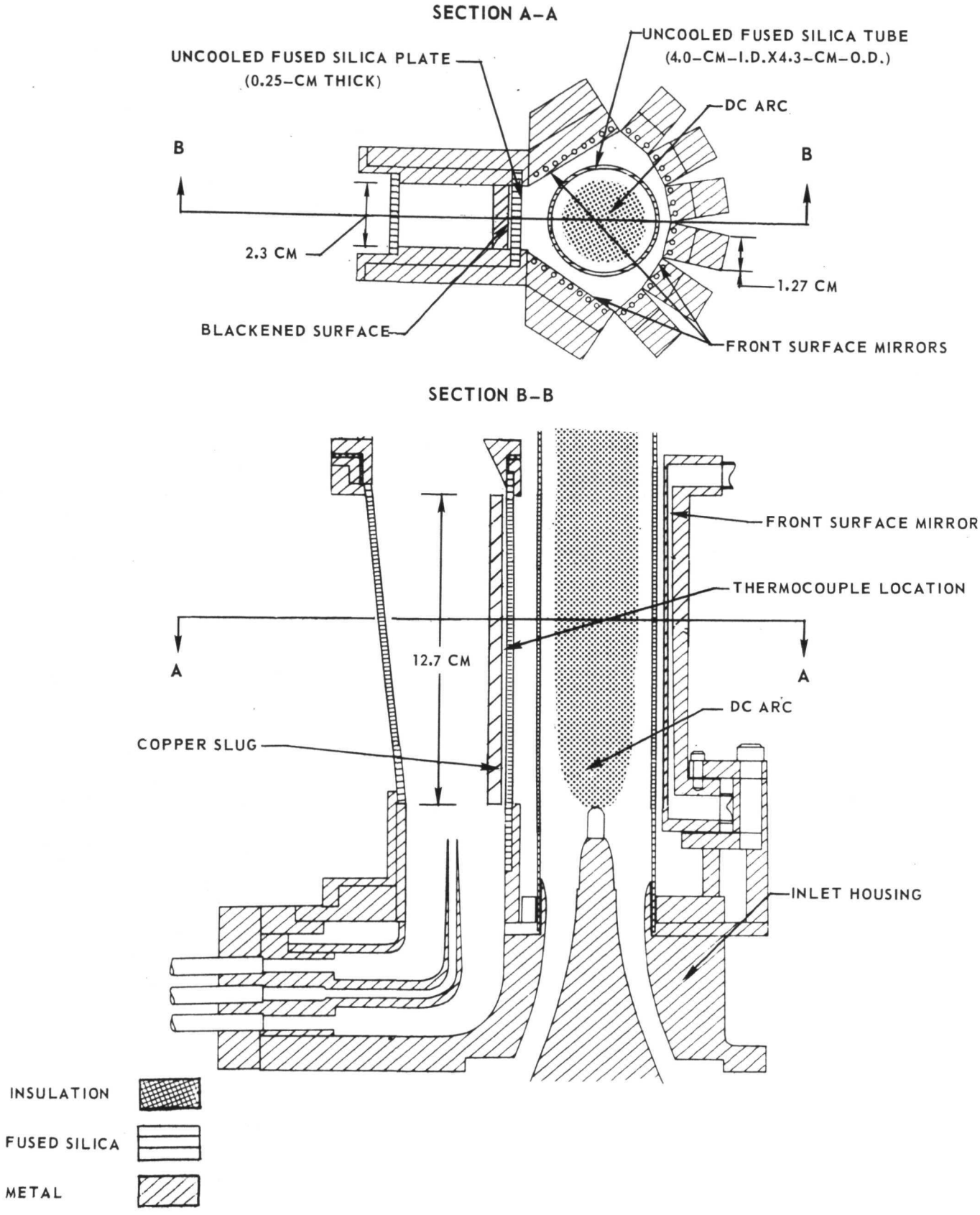

FIG. 14

EFFECT OF SEGMENTED MIRROR ASSEMBLY ON RADIANT FLUX INCIDENT ON TEST SECTION

TESTS AT DC ARC POWERS UP TO ABOUT 100 KW

SEE FIGS. 12 AND 13 FOR TEST CONFIGURATIONS

TEST SECTION AREA = 29 CM^2

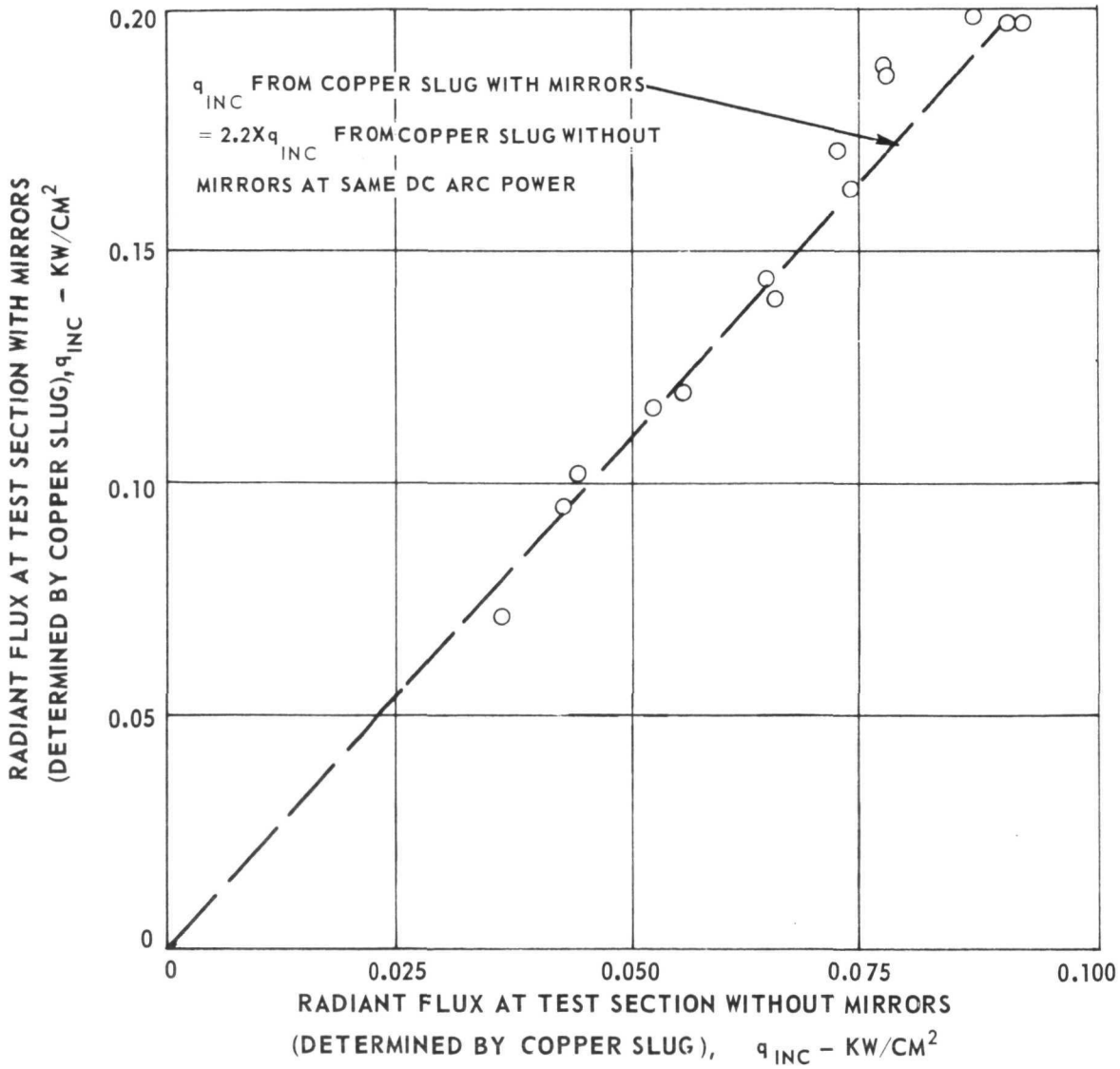

VARIATION OF BULK EXIT TEMPERATURE WITH RADIATION INCIDENT ON TEST SECTION FOR TESTS WITH REFLECTOR IN REAR OF PROPELLANT DUCT

SEE FIGS. 9 AND 10 FOR TEST CONFIGURATION

SEE TABLE I FOR FURTHER DETAILS OF DATA

SYMBOL	ARGON WEIGHT FLOW, $\dot{m}_A$ – G/SEC	TUNGSTEN WEIGHT FLOW, $\dot{m}_W$ – G/SEC
○	2.2	7.0
◑	4.4	7.0
●	8.8	7.0
□	8.8	5.0 AND 5.5

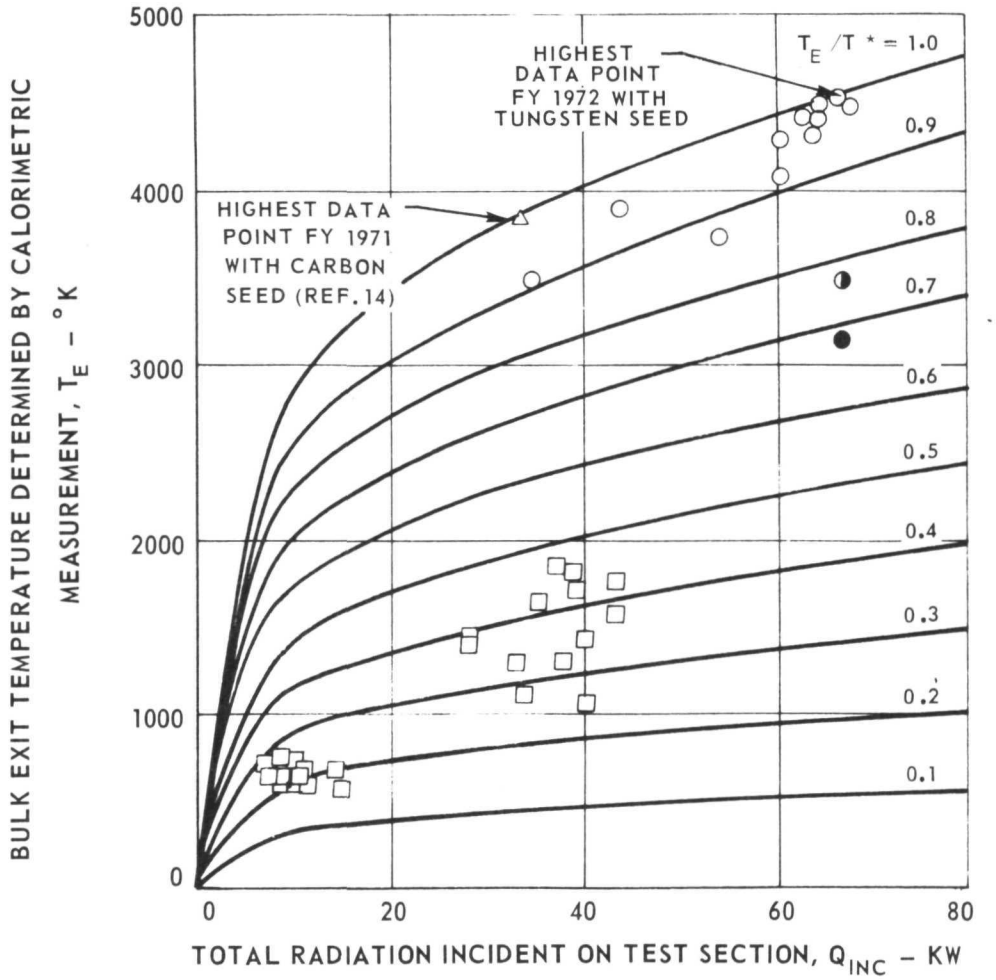

VARIATION OF BULK EXIT TEMPERATURE WITH RADIATION ABSORBED BY PROPELLANT FOR TESTS WITH REFLECTOR IN REAR OF PROPELLANT DUCT

SEE FIGS. 9 AND 10 FOR TEST CONFIGURATION

SEE TABLE I FOR FURTHER DETAILS OF DATA

SYMBOL	ARGON WEIGHT FLOW, $\dot{m}_A$ – G/SEC	TUNGSTEN WEIGHT FLOW, $\dot{m}_W$ – G/SEC
○	2.2	7.0
◑	4.4	7.0
●	8.8	7.0
□	8.8	5.0 AND 5.5

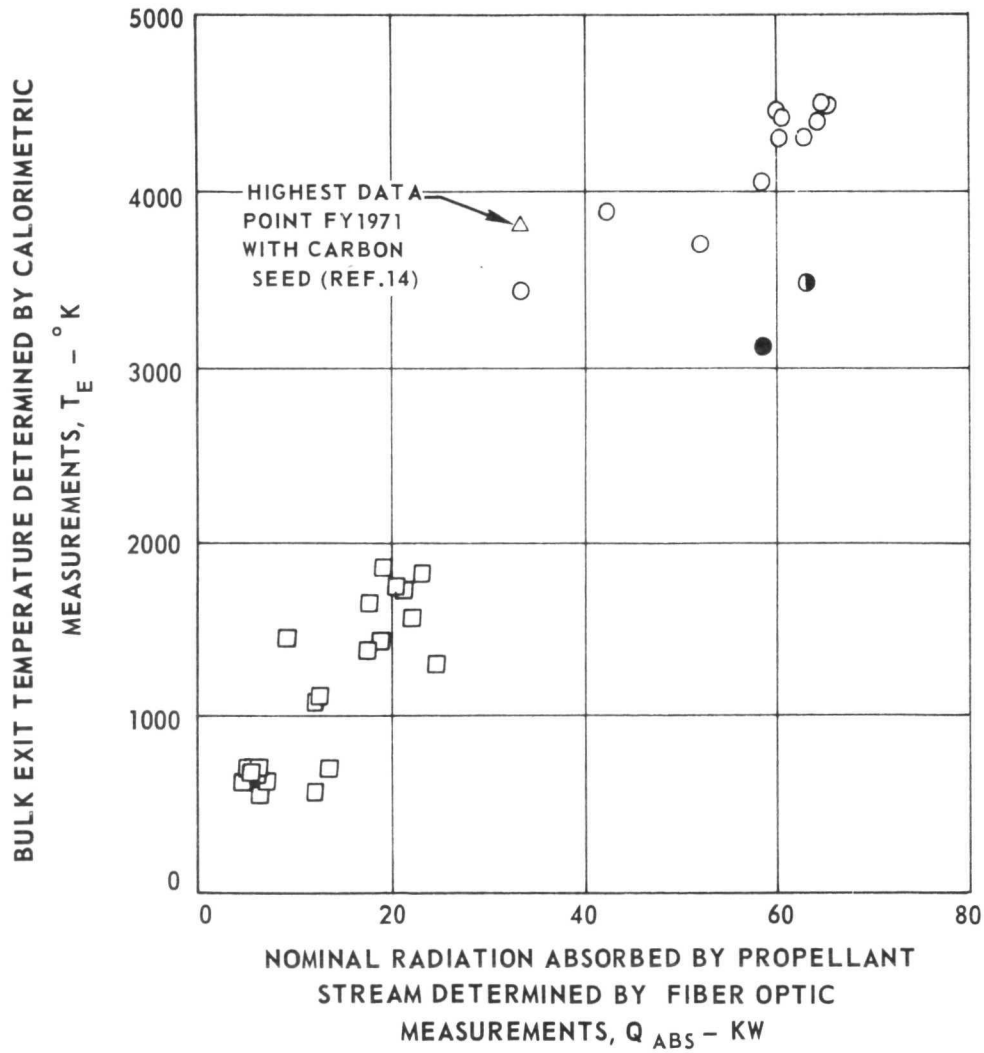

CALCULATED VARIATION OF BULK EXIT TEMPERATURE WITH POWER DEPOSITED IN GAS FOR DIFFERENT SEED WEIGHT FLOW RATES

$\dot{m}_A$ = ARGON WEIGHT FLOW RATE, 8.8 G/SEC (CONSTANT)

$\dot{m}_W$ = TUNGSTEN WEIGHT FLOW RATE, G/SEC (VARIED)

$Q_{GAS} = Q_{ABS} - Q_{LOST}$ (SEE TEXT)

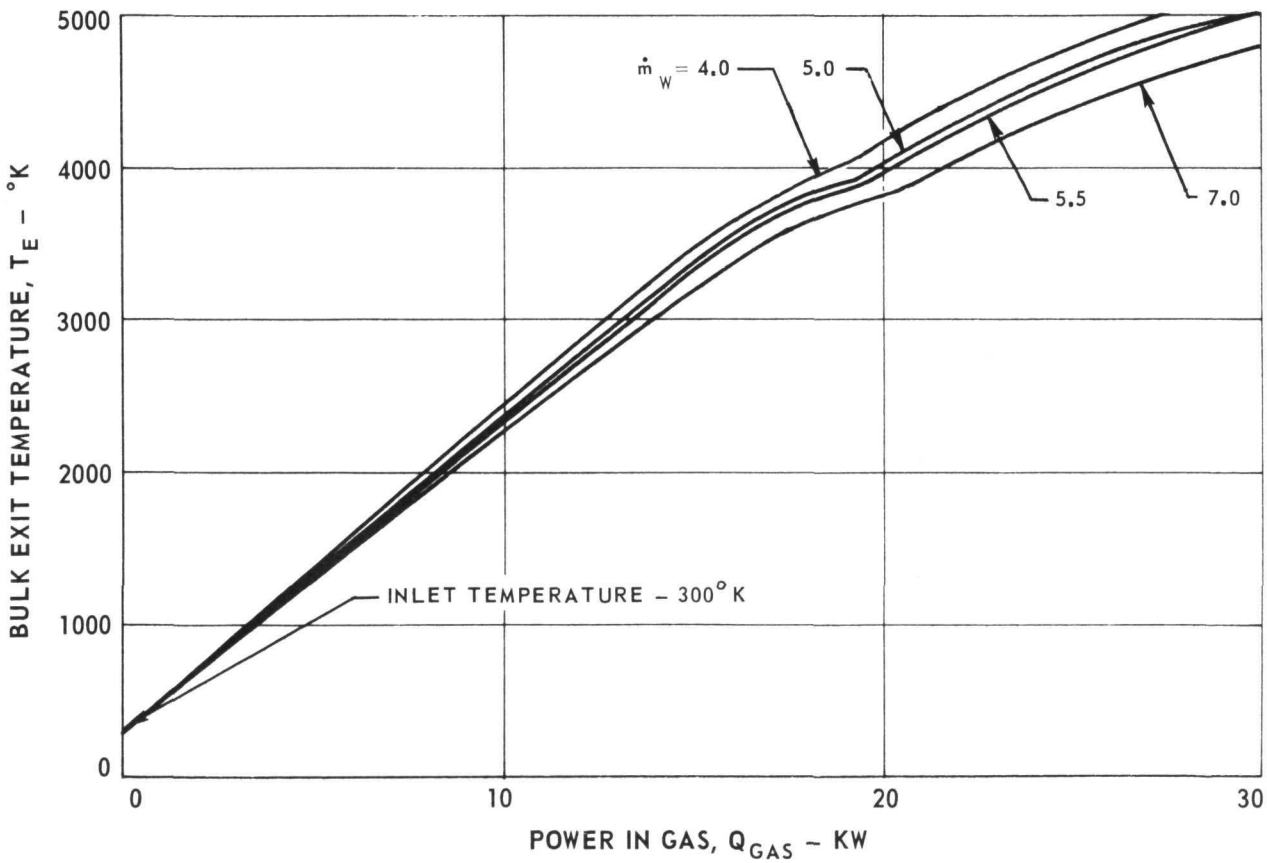

CALCULATED VARIATION OF BULK EXIT TEMPERATURE WITH POWER DEPOSITED IN GAS FOR DIFFERENT ARGON FLOW RATES

$\dot{m}_W$ = TUNGSTEN WEIGHT FLOW RATE, 7.0 G/SEC (CONSTANT)

$\dot{m}_A$ = ARGON WEIGHT FLOW RATE, G/SEC (VARIED)

$Q_{GAS} = Q_{ABS} - Q_{LOST}$ (SEE TEXT)

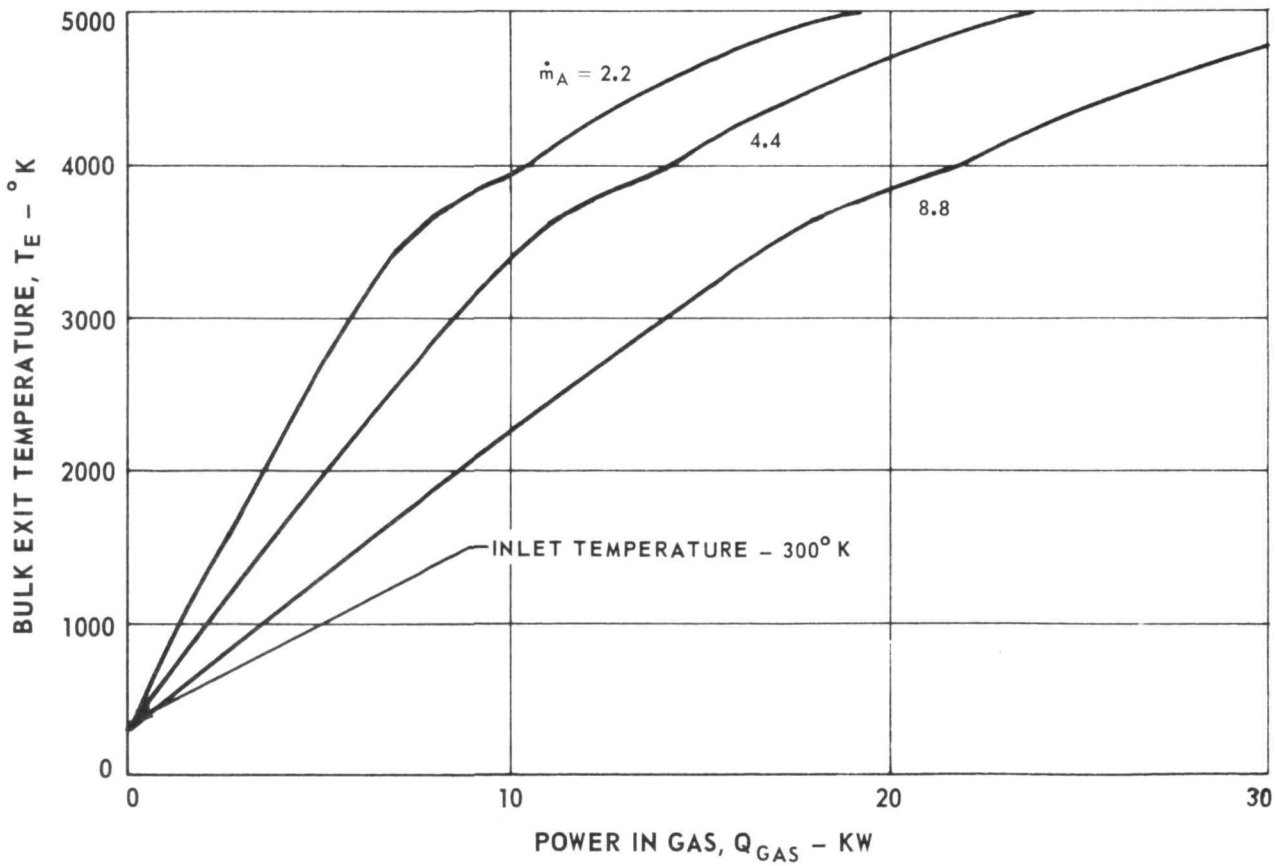

FIG. 19

RESULTS OF PROPELLANT HEATING TESTS WITHOUT REFLECTOR IN REAR OF PROPELLANT DUCT

SEE TABLE I FOR FURTHER DETAILS OF DATA

$\dot{m}_A$ = ARGON WEIGHT FLOW RATE, 8.8 G/SEC

$\dot{m}_W$ = TUNGSTEN WEIGHT FLOW RATE, 4.0–5.5 G/SEC

a) VARIATION OF BULK EXIT TEMPERATURE WITH INCIDENT RADIATION

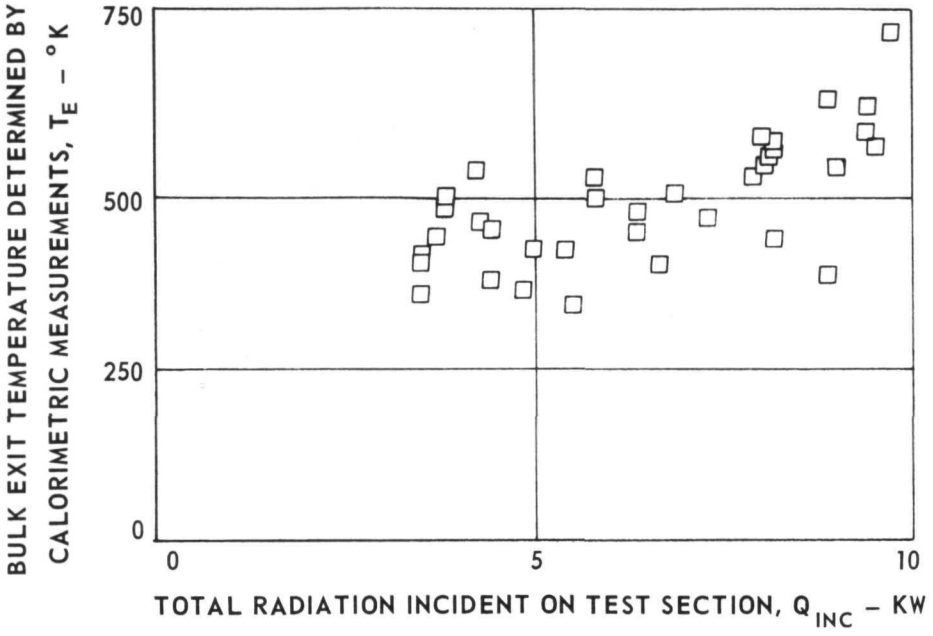

b) VARIATION OF BULK EXIT TEMPERATURE WITH RADIATION ABSORBED BY PROPELLANT

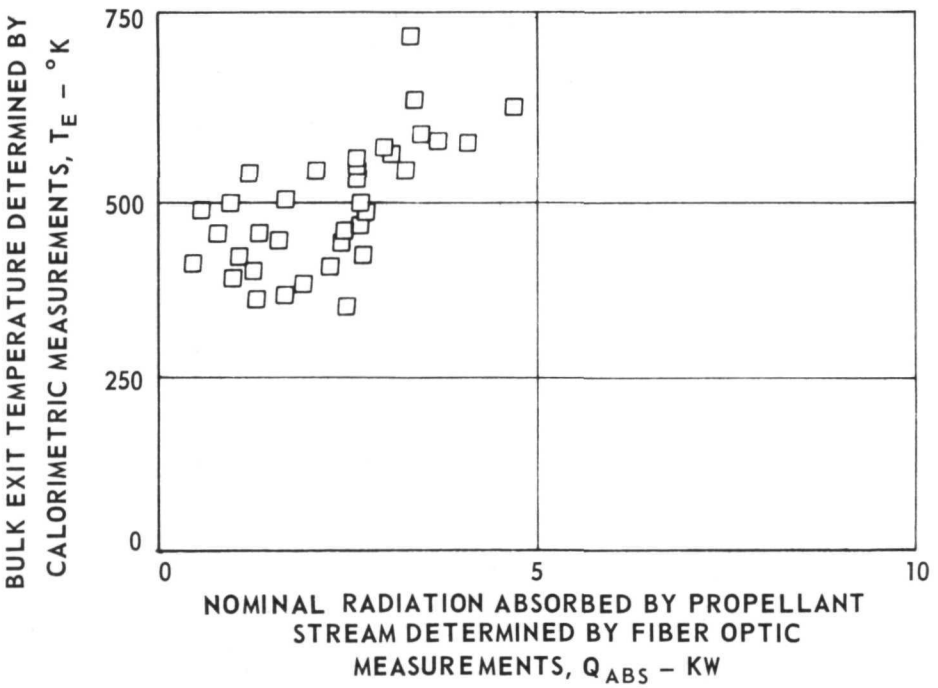

PHOTOGRAPHS OF ROTATING DRUM POWDER FEEDER

SEE FIG. 6 FOR FLOW SYSTEM

(a) DRUM INTERIOR FROM OUTLET END (END PLATES REMOVED)

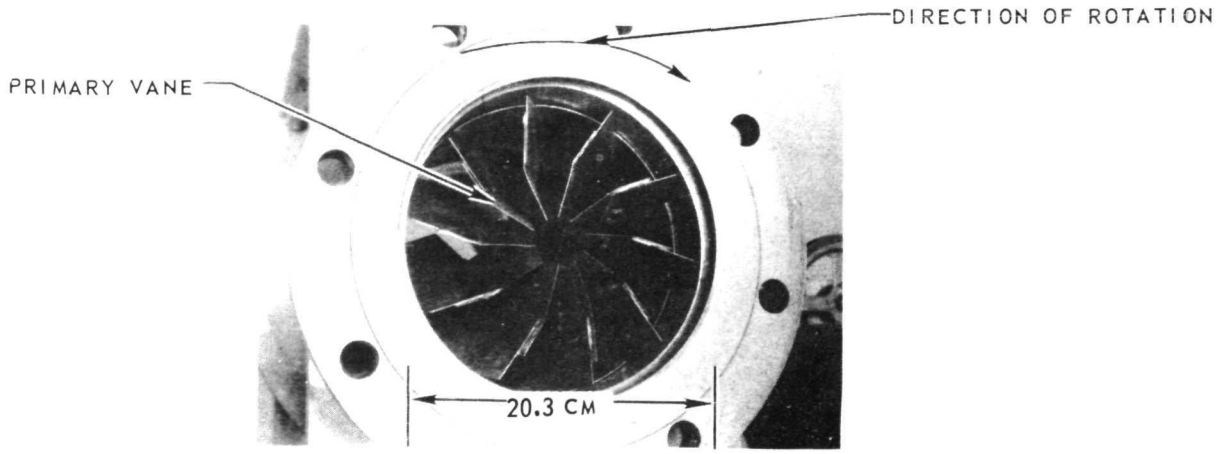

(b) POWDER FEEDER ASSEMBLY

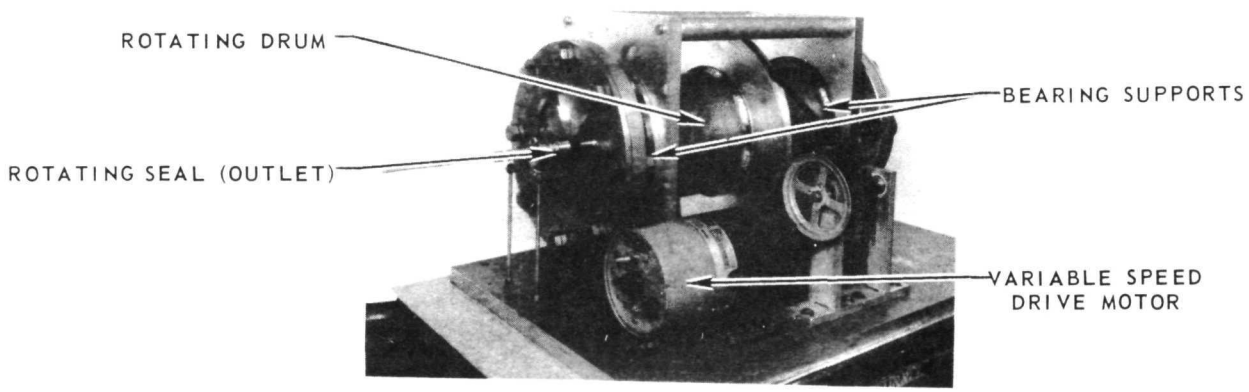

(c) DRUM INTERIOR FROM INLET END (END PLATES REMOVED)

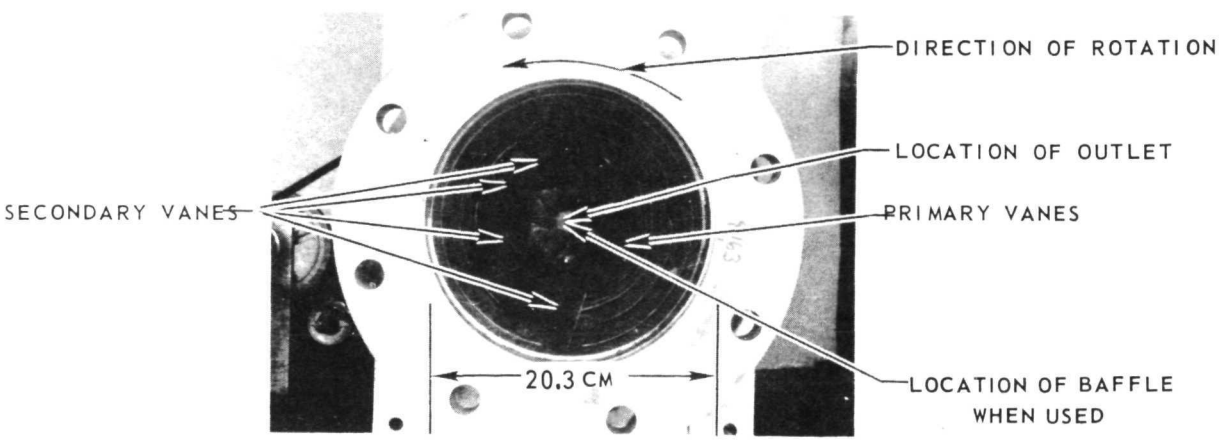

GEOMETRY OF PRIMARY POWDER FEEDER VANES

SEE FIG. 20 FOR COMPLETE ASSEMBLY

ALL DIMENSIONS IN CM

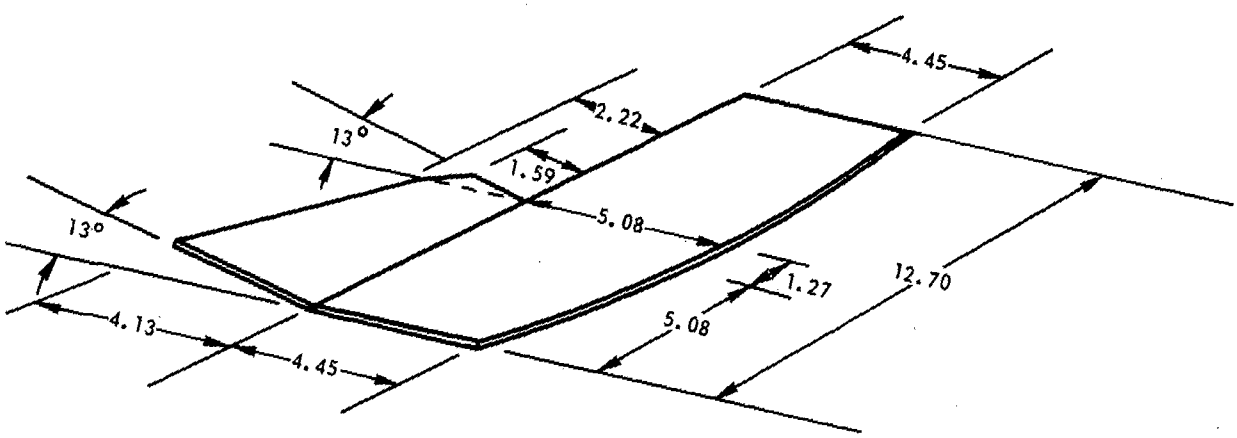

VARIATION OF AVERAGE TUNGSTEN WEIGHT FLOW WITH AVERAGE PRESSURE IN POWDER FEEDER FOR VARIOUS ORIFICE DIAMETERS - WITHOUT BAFFLE

SYMBOL	NOMINAL ORIFICE DIAMETER -CM
△	0.079
□	0.139
○	0.198

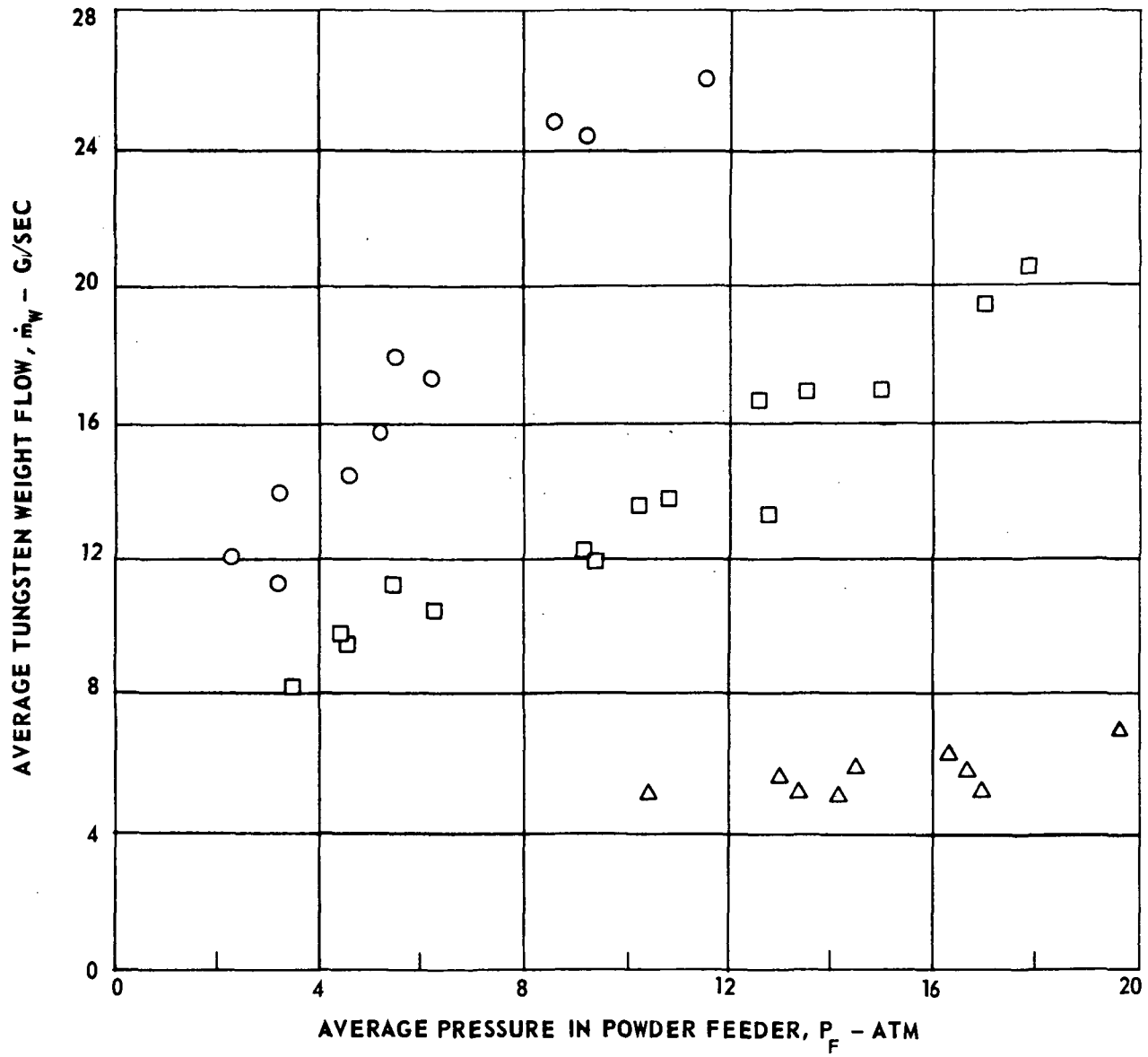

VARIATION OF AVERAGE TUNGSTEN WEIGHT FLOW PER UNIT AREA WITH AVERAGE PRESSURE IN POWDER FEEDER FOR VARIOUS ORIFICE DIAMETERS - WITHOUT BAFFLE

SYMBOL	NOMINAL ORIFICE DIAMETER —CM
△	0.079
□	0.139
○	0.198

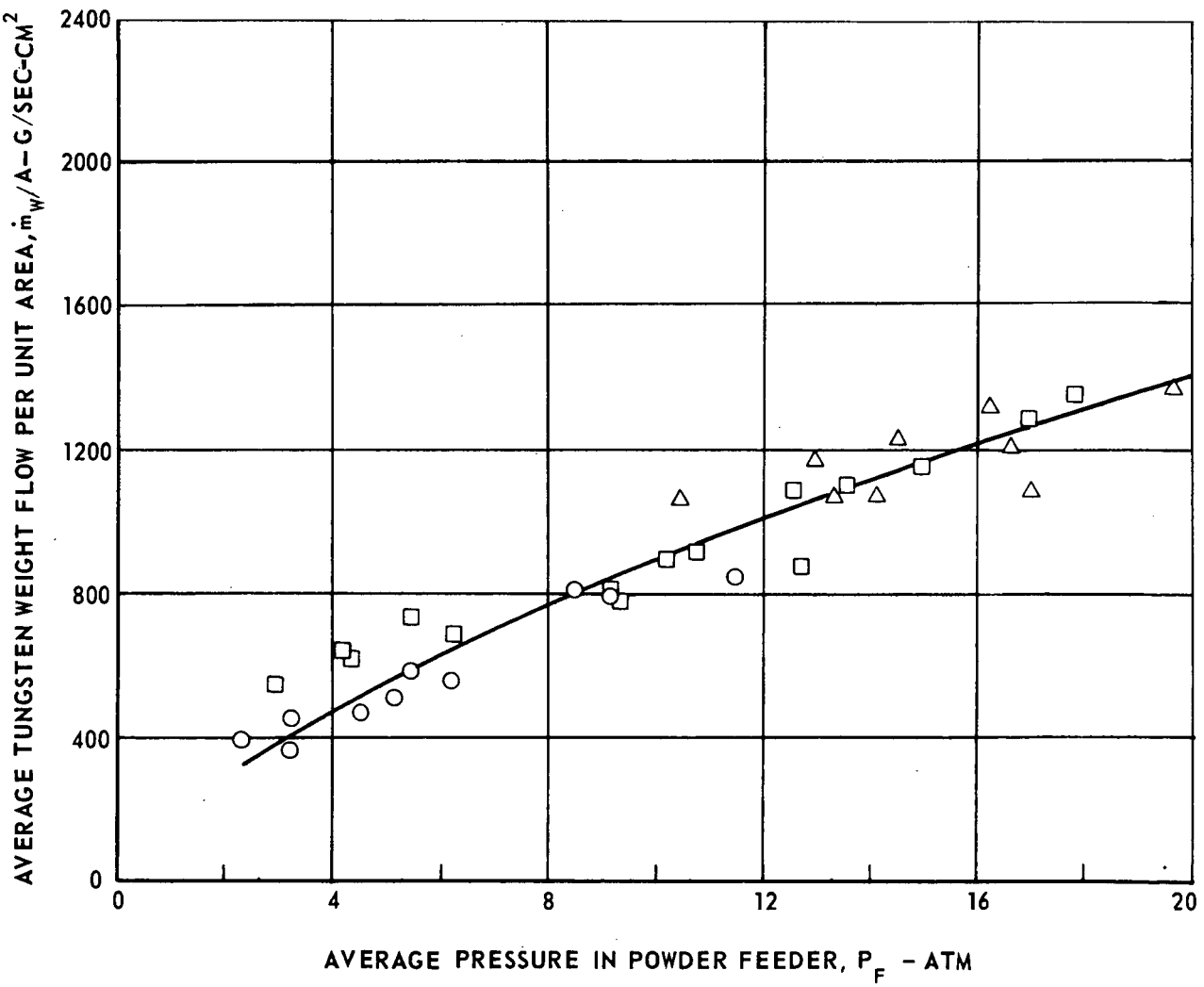

FIG. 24

VARIATION OF AVERAGE TUNGSTEN WEIGHT FLOW WITH WEIGHT OF TUNGSTEN IN POWDER FEEDER – WITHOUT BAFFLE

0.139-CM NOMINAL ORIFICE DIAMETER

APPROXIMATELY 13 ATM AVERAGE PRESSURE

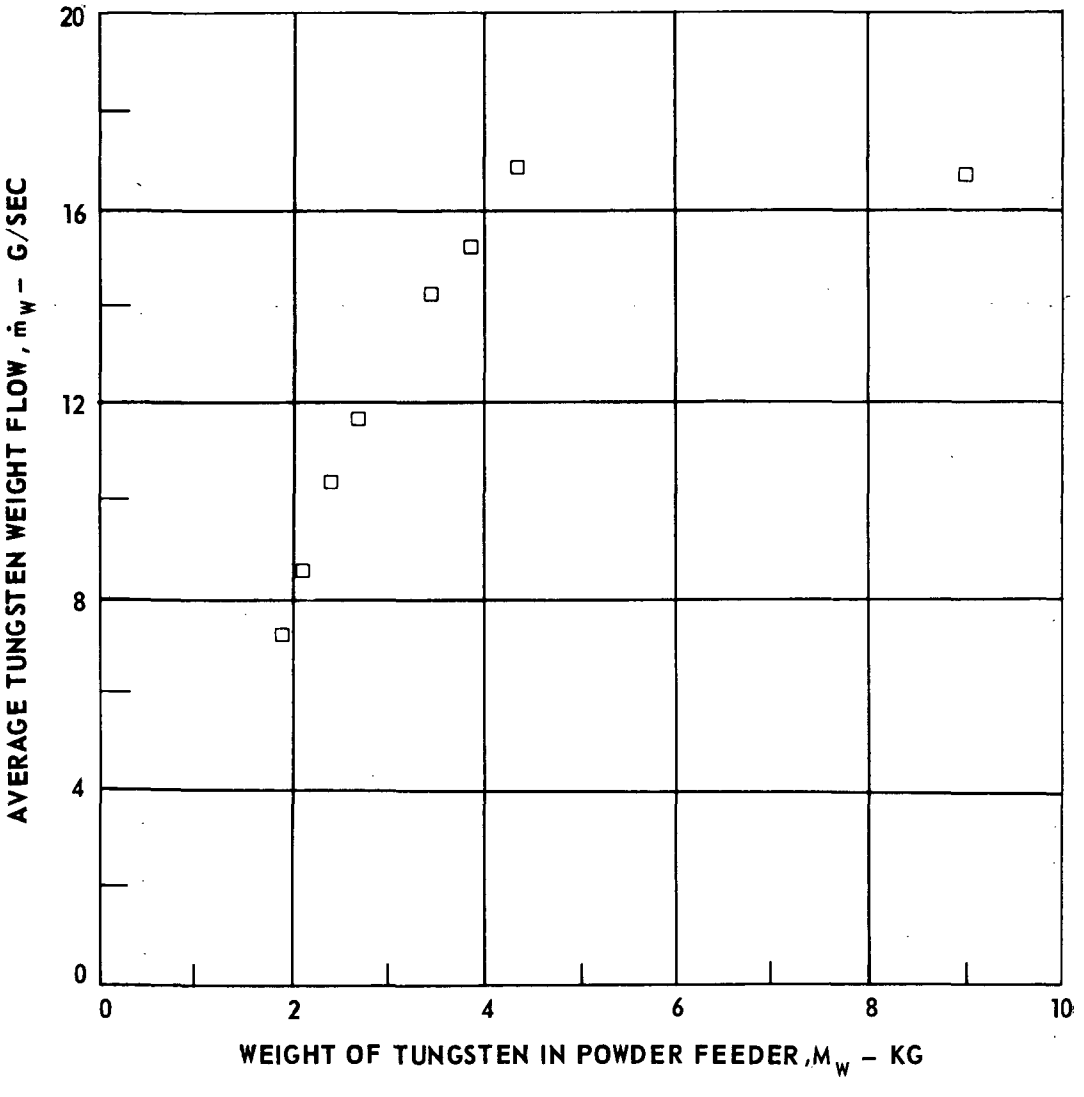

FIG. 25

VARIATION OF AVERAGE TUNGSTEN WEIGHT FLOW PER UNIT AREA WITH AVERAGE PRESSURE IN POWDER FEEDER FOR VARIOUS ORIFICE DIAMETERS – WITH BAFFLE

SYMBOL	NOMINAL ORIFICE DIAMETER – CM
△	0.079
◇	0.094
▽	15.24– CM-LONG X 0.165 – CM-I.D. TUBE

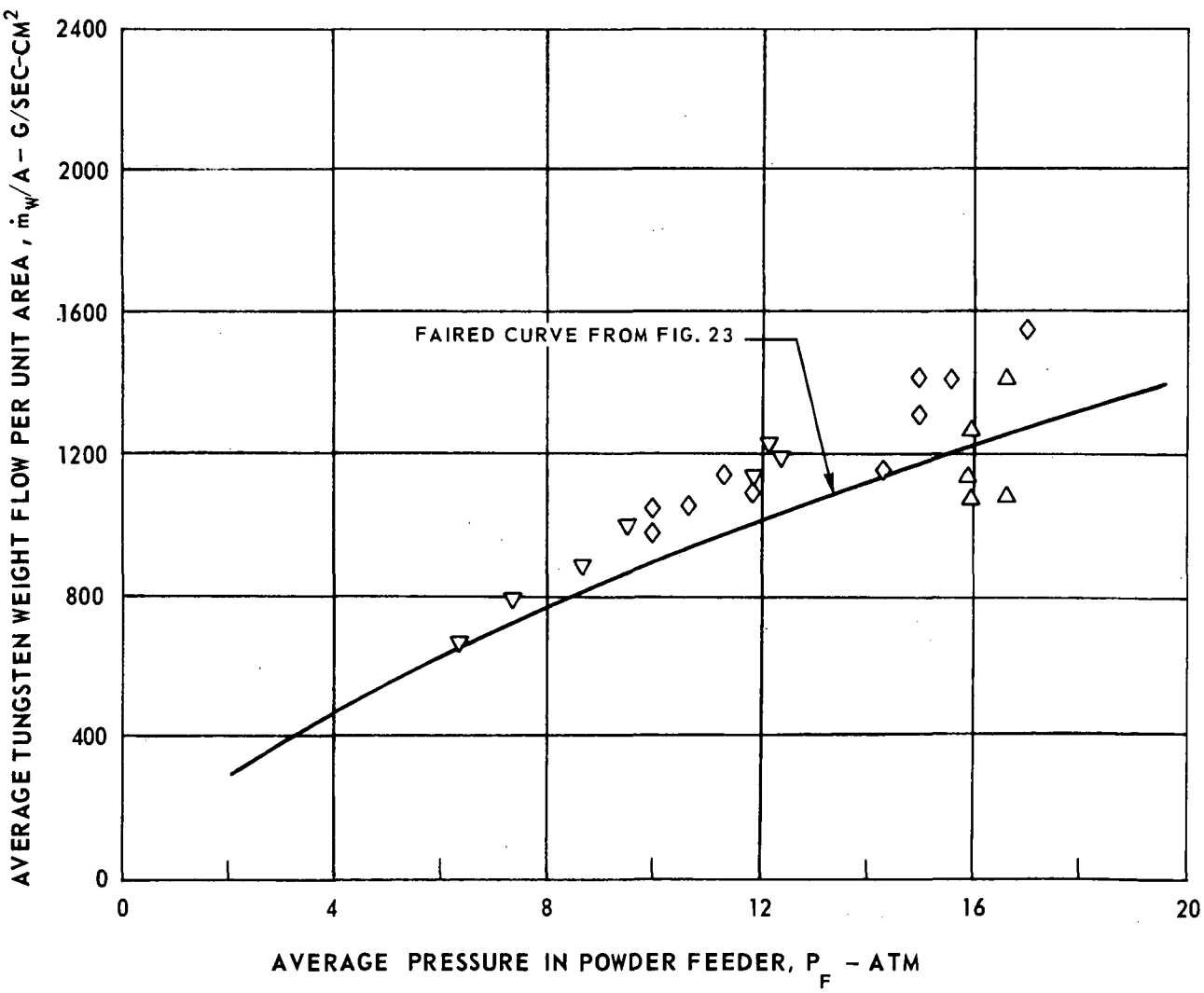

United
Aircraft
Research
Laboratories

UNITED AIRCRAFT CORPORATION

EAST HARTFORD, CONNECTICUT 06108